CHAPTER 5

Formation of Polymeric Hydrogenated Carbon Nitride Films

5 FORMATION OF POLYMERIC HYDROGENATED CARBON NITRIDE THIN FILMS

5.1 Introduction

This chapter presents studies on the fabrication and characterization of polymeric hydrogenated carbon nitride thin films (p-CN_x:H) deposited using the home-built radio frequency plasma enhanced chemical vapour deposition (rf PECVD) at an electrode distance (D_E) of 5 cm. This distance is chosen instead of 6 cm since it was observed that films deposited at 6 cm tended to form dust particles which settled on the film surface. Also since most of the characteristics of the film, which include the PL, E_{04}, FTIR spectra and growth rate, remain almost the same for D_E of 6 and 5 cm, the uniformity and consistency in growth structure for 5 cm (where the deposited films are almost dust-free) is preferred.

While the studies of the nanostructured CN_x:H film concentrates on the structural characteristics of the film (i.e. the growth and formation of its vertical aligned structures), the studies of these p-CN_x:H focus on their structural and optical characteristics. Also the thermal stability of these films was ascertained. In short, the objectives of these studies include:

(i) The effect of radio frequency (rf) plasma discharge power and the determination of optimized rf power for the sequential studies

(ii) The studies of bonding characteristics and the structural evolution as a function of nitrogen incorporation

(iii) The thermal stability together with the structural and PL degradation of these films.

The first and second objectives were carried out through the studies of the effects of applied rf power and nitrogen-to-methane flow-rate ratio on the properties of the deposited CN_x:H films. Each study is presented separately in two sequential sections beginning with the variation in rf power. Efforts to correlate these parameters to their PL characteristics were undertaken. From these results, the optimized range for the fabrication of p-CN_x:H with highest PL emissions was also determined. The third objective was undertaken through the effect of thermal annealing on the p-CN_x:H films obtained from these optimized deposition conditions. The structural changes were studied and the effects of thermal annealing and the changes in chemical bonding and PL characteristics were determined.

As compared to Chapter 4, the characterization and analytical methods used here are relatively simpler. The films were characterized by means of surface profilometer, optical measurements employing a UV-Visible near-infrared (UV-Vis-NIR) spectroscopy, Auger electron spectroscopy (AES), Raman scattering, Fourier transform infrared spectroscopy (FTIR) and Photoluminescence measurement. Thus these measurements provide four main properties which include the film thickness, optical characteristics, chemical composition and chemical bonding characteristics.

5.1.1 Growth mechanism postulated

Before the actual results are presented, it is deemed necessary to form a general model for the growth mechanism of the CN_x:H films deposited by this rf PECVD technique. Since plasma processing and in-situ studies of the film growth in the chamber were not part of the focus of this work, the growth mechanism of these film were postulated from referential work carried out on similar deposition systems.

To adopt a suitable growth mechanism, it is important to consider the type of deposition method used and the type of film produced. Among the many available models, the 'subplantation' process of hyperthermal species was deems the closest related to this work. Subplantation refers to the process of low energy subsurface implantation (Robertson 2002a), while hyperthermal species are produced from the plasma in PECVD. Lifshitz and co-workers (Lifshitz et al. 1989; Lifshitz et al. 1990; Lifshitz et al. 1994) have studied various aspects of film growth from hyperthermal species and have proposed that when such species incident on a substrate the following might occur:

(a) Penetration of impinging species into subsurface layers of the substrate. The depth of the penetration and distribution depends on the properties of the impinging species and targeted substrate.
(b) Stopping of the energetic species in the substrate via a three energy lost mechanism which include atomic displacements, phonon excitations and electron excitation.
(c) Site occupation of these species. This progresses from their initial stopping in the substrate which is determined by the host matrix that acts as a "mold" for its

structure, towards further displacement or reallocation due to collision with ensuing impinging energetic species, or due to re-crystallization induced by compositional changes during the deposition process.

(d) Phase formation due to the increase in the concentration of penetrating species in the host matrix. This will result in the inclusion of new phases, accompanied by outward expansion of the substrate layer.

(e) Evolution in the surface composition whereby in the early stages, the surface composition is made up mostly of the substrate materials. As the growth progresses, due to gradual sputtering and/or dilution of ion-mixing mechanism, the surface would finally consist purely of the impinging species.

(f) Evolution of the film structure. This is influenced by a number of aspect which includes the "mold" effect of the host matrix, preferential displacement of atoms due to collisions and diffusion rates of vacancies and interstitials created during the deposition.

(g) Oriented and crystalline growth, which is attributed to epitaxial growth and/or preferential orientation of the film due to the influence of the crystallinity of its under-layer surface.

(h) Re-sputtering yield of both substrate and trapped atoms by the impinging species determines whether film growth occurs. It is necessary for the sputtering yield to be low for efficient deposition to occur.

As studies on this model progresses, emphasis was put on subplantation process involving steps (a) to (d) especially on the growth of carbon films which focuses on the variation in the amount of sp^2 and sp^3 bonding configuration. While Lifshitz et al. (Lifshitz et al. 1990) argues that sp^3 sites accumulate by preferential displacement of sp^2 sites, more recent studies particularly that of Robertson (Robertson 2002a) proposed

that preferential displacement is not the determining factor in the inclusion of sp^2 and sp^3. Instead the subplantation creates metastable increase in density which causes such preference.

The subplantation model proposed by Robertson (Robertson 2002a) using carbon ions as the species impinging onto an amorphous carbon surface with energies in the range of 10-1000 eV, is taken into consideration. These ions have a penetration range of only few nm. The ion range increases with the increase in ion energy, and allows the ion to penetrate deeper into the solid at high energy. A small fraction is used to penetrate the surface, and another small fraction to cause atom displacements. The rest of the energy is dissipated as phonon which involves three stages made up of a collision stage, a thermalization stage and relaxation stage.

Schematics of the film growth model and the relaxation stage are shown in Figure 5.1 and Figure 5.2 respectively. Incident ion with low energy will not have enough energy to penetrate the surface. Instead it will stick to the surface and remain at its lowest energy state which is sp^2. On the other hand, if the ion energy is higher that the penetration threshold of the surface, it can penetrate and enter a subsurface interstitial site. The resulting increase in local density will cause the local bonding around the atom to reform. This is fuelled by the thermalization process where the ion looses energy to its surroundings through phonon and electron excitations. These two energy dispersion is referred as “thermal spikes” (Lifshitz et al. 1990; Lifshitz et al. 1994). The model also assumes that highly energetic conditions of ion bombardment occur during film growth and atomic hybridization is strongly influence by the changes in local density. The bonding tends towards sp^2 at low density and sp^3 when the density is high.

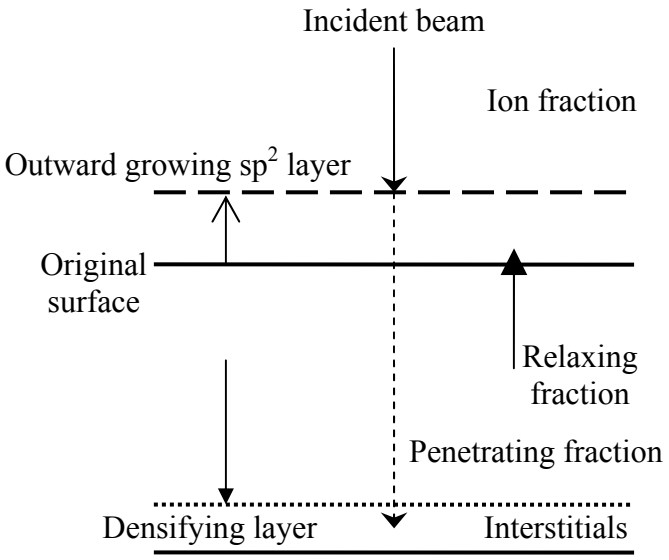

Figure 5.1 Schematic diagram of densification by subplantation (Robertson 2002a)

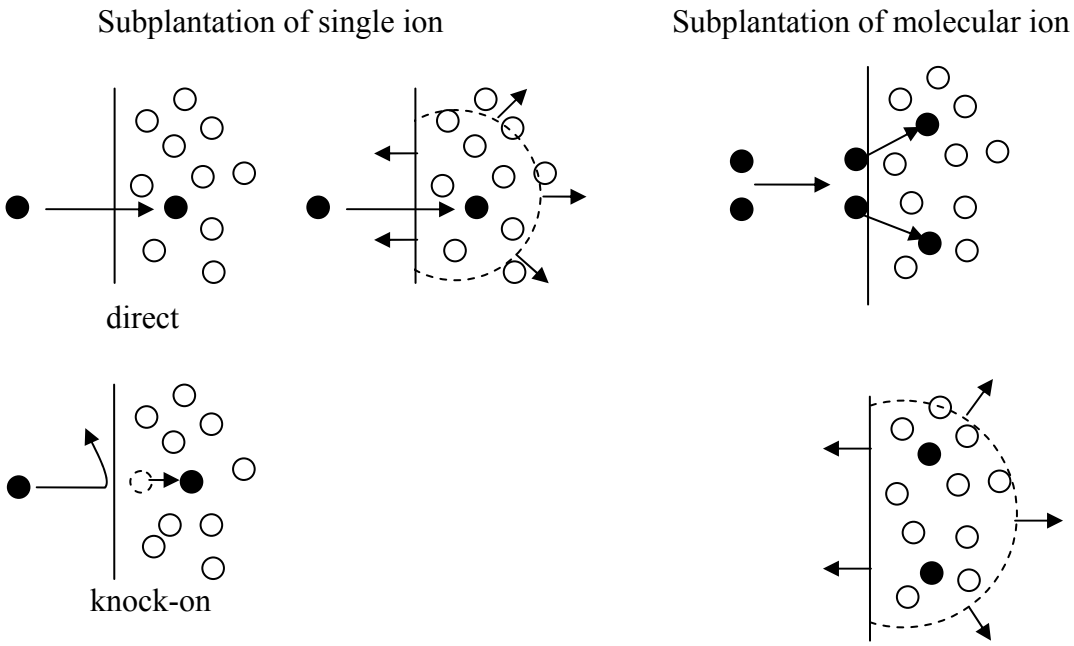

Figure 5.2 Schematic of the penetration and relaxation stage for cases of single and molecular impinging ions.

This subplantation model is one of the three general stages in plasma deposition (Robertson 2002a). To get a complete model, it is also important to consider the other two stages which are made up of the reaction in the plasma (dissociation, ionisation etc.)

and the plasma-surface interaction. The plasma reactions are driven by energetic electrons. Other species may also form in secondary reactions in the plasma to produce polymerisation. The plasma species incident on the growing surface consists of ions and neutrals. The interaction of the ions results in the subplantation process discuss earlier. The neutral species including un-dissociated precursor gas, mono-radicals such as CH_3 and other unsaturated species such as C_2H_4, C_2H_2, etc do not penetrate the surface but instead may stick to the film surface to increase the outward growth. Contribution of these neutral species depends on their sticking probability. Higher order unsaturated species such as di-radicals reacts strongly with the film surface and may be inserted directly into surface C-C or C-H bonds (Robertson 2002a). The mono-radical, CH_3 can only react with the film surface through the presence of dangling bonds and may react to form C-C bonds. These dangling bonds may be created through H removal by displacement by impinging ions or H-H abstraction (which forms desorbed H_2). The presence of high atomic H in CH_3 compensates the low sticking probability of CH_3 making such this species important in the growth of the film.

Impinging hydrogen atoms and ions reacts slightly different from hydrocarbon species. H atoms are small enough to penetrate up to 2 nm into the film and could abstract H from C-H bonds in the film and create subsurface dangling bonds. Additionally because of their low mass, H^+ ions have long range and can penetrate deeply into the film. These ions may create or re-saturate dangling bonds deep in the film.

In this work the growth mechanism of the polymeric CN_x:H films is slightly different since a mixture of methane and nitrogen is used. The effects of nitrogen dilution in such CH_4 + N_2 mixtures have been of keen interest to many researchers

(Bouzerar et al. 2005; Conway et al. 2000; Kaufman et al. 1989; Lejeune and Benlahsen 2008; Majumdar et al. 2007; Tanarro et al. 2007; Wang et al. 2006b), especially since it is this aspect which contributes to the growth of a variety of thin CN_x:H film structures. The presence of nitrogen would have a significant effect on the plasma and film growth. For intense nitrogen discharges, N atoms and CN radicals are said to be the main precursors leading to the formation of amorphous a-CN_x:H films (Alibart et al. 2008b; Kaltofen et al. 1997; Valentini et al. 2001a). With the increase in relative content of N_2, ionic and atomic N bombardment will increase inducing an increase in chemical sputtering (Davis and et al. 1987; Hao et al. 2007; Motta and Pereyra 2004; Singh et al. 2010). This will compete with chemisorbed gas-phase radicals on the dangling bonds which is the main radical sites on the films surface. These bonds are created from the impinging ionic species on the growth surface whereby these species are part of the product of the decomposition of CH_4 and N_2 molecules (apart from the neutral radicals and atomic or ionic species) (Denton et al. 1972).

5.2 Effects of Radio-Frequency Power on the Properties of Polymeric CN_x:H.

This is the first optimization section which aims to determine the effects of radio frequency power (P_{rf}) on the deposition of the p-CN_x:H films and from there to determine the optimized P_{rf} value or range for the highest PL emission. The progression of this current section is shown in the flow chart depicted in Figure 5.3.

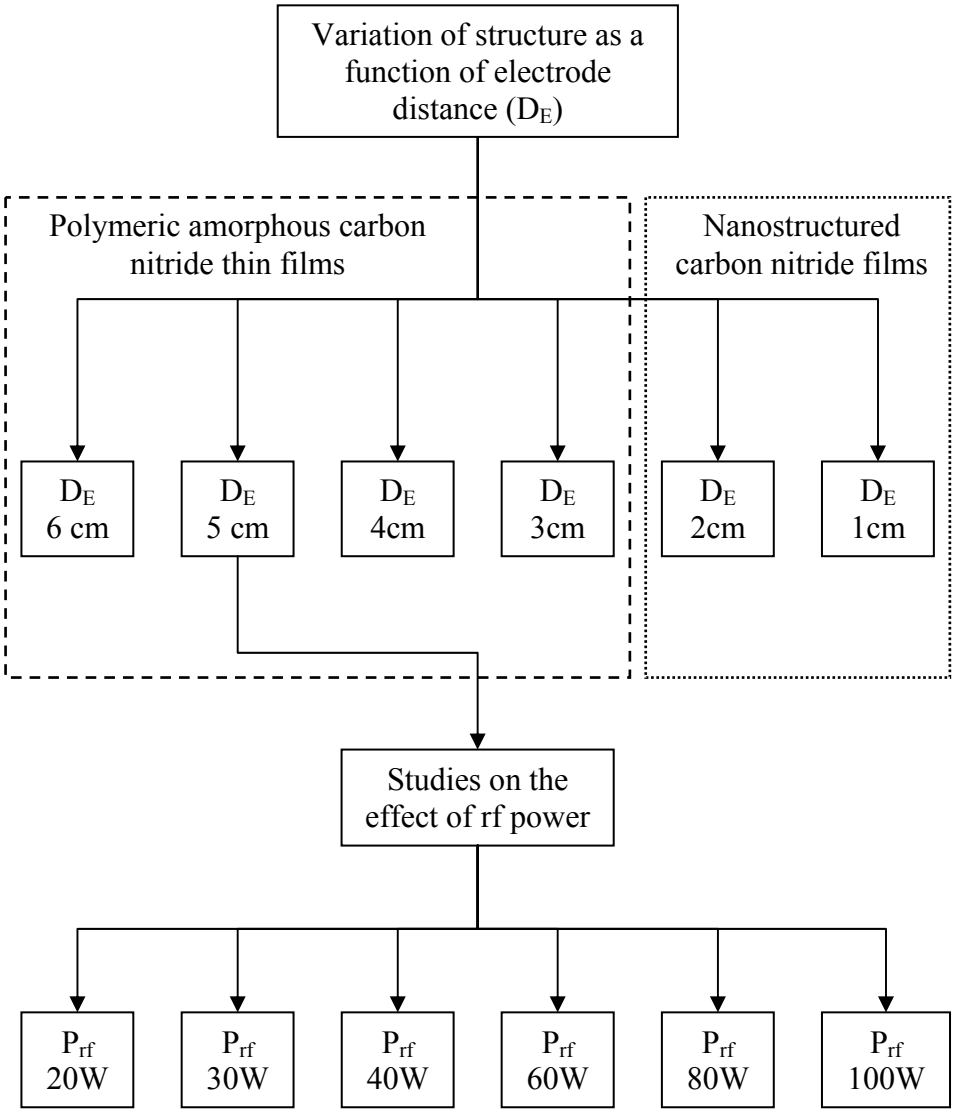

Figure 5.3: Flow chart showing the progression of the current studies of p-CN_x:H films

What is most interesting about this part of the work is that although the choice of applied rf power is crucial for the determination and control of CN thin film depositions using rf PECVD, relatively few studies or publication are available. Even closely related publication such as those of Mutsukura and Akita (Mutsukura and Akita 2000) and Yu et. al, (Yu et al. 2002b) only give a general description on these effects.

Apart from the UV-Vis NIR measurements which were done for film deposition on quartz substrates, all other characterizations were carried out for films deposited on (111) p-type silicon substrates. P_{rf} which drives the plasma generation in the chamber was varied between 20 -100 W. 100W was set as the maximum limit due to the constraints and stability of the home-built rf PECVD system. All other parameters, as listed in Table 5.1, were kept constant.

Table 5.1: Deposition parameters for the study on the effects of applied rf power on the structural properties of p-CN_x:H thin films.

	Parameter	Set values					
1.	rf power *	20 - 100 W					
	Power (W)	20	30	40	60	80	100
	Power Density (W/cm^2)	0.25	0.38	0.51	0.76	1.02	1.27
2.	Electrode distance	5 cm					
3.	Initial substrate temperature	100°C					
4.	Chamber base pressure	~$1x10^{-5}$ mbar					
5.	Methane (CH_4) mass flow-rate	20 sccm					
6.	Nitrogen (N_2) mass flow-rate	60 sccm					
7.	[N_2/(N_2+CH_4)]	0.75					
8.	Deposition time	60 minutes					
9.	Deposition pressure	0.8 mbar					

*indicates the variable parameter for the study

5.2.1 Determination of growth rate measured by surface profilometry

The variation in film growth rate as a function of P_{rf} is as shown in Figure 5.4. The growth rate increases almost linearly as P_{rf} increases. This is attributed to an increase in reactive gas dissociation which in turn increases the generation of ionic and/or neutral radicals which would contribute to the growth of the film. The increasing trend indicates that the chemisorbed C, CN and N species dominate the growth process as compared to the etching effect and H passivation.

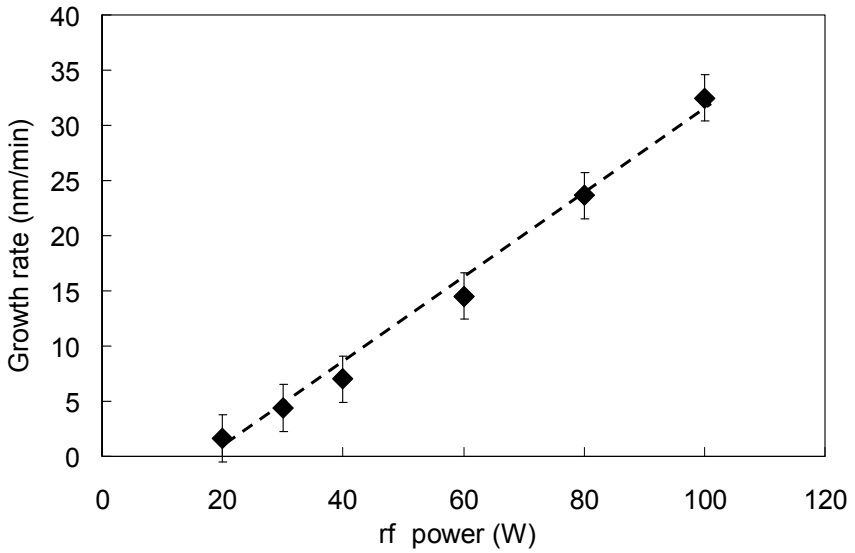

Figure 5.4: Variation of growth rate as a function of applied rf power.

Line is as guide to the eye.

5.2.2 Optical properties measured by UV-Vis NIR spectroscopy

From the optical measurements carried out using the UV-Vis NIR spectroscopy, the optical energy gap, E_{04} and refractive index, n are calculated. E_{04} was determined in the way described in Chapter 4, while here, an additional variable, the refractive index, n is introduced. The variations in E_{04} and n as a function of P_{rf} is shown in Figure 5.5.

The values of E_{04} and n for films deposited at P_{rf} of 20 W could not be determined since the film was too thin which result in the lack of interference fringes and clearly defined absorption edge.

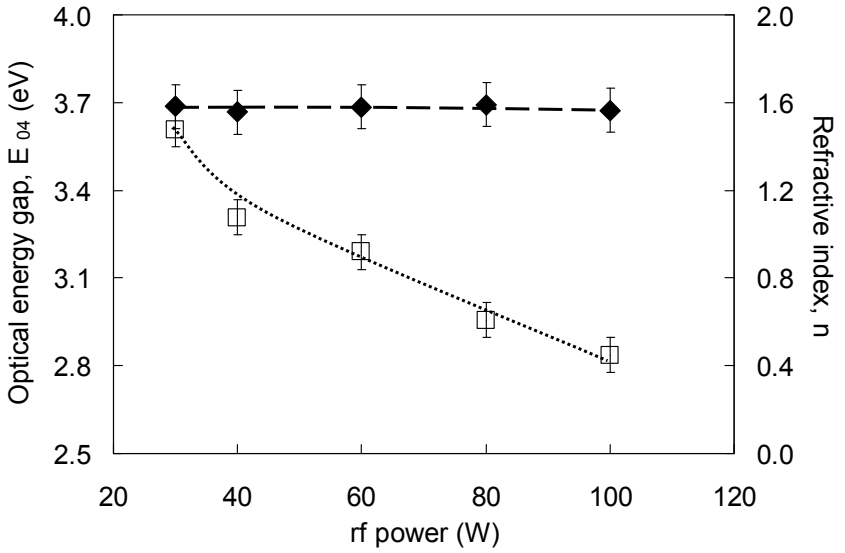

Figure 5.5: Variation of optical energy gap (□) and refractive index (♦)

as a function of applied rf power. Line is as guide to the eye.

E_{04} decreases almost linearly with the increase in P_{rf} in the range of 30-100 W. In contrast, n remains almost constant within this range. The change in E_{04} without a corresponding change in n is an indication of a modification of the states within the energy gap (Khan et al. 1999). The decrease in E_{04} is associated to the broadening of the localized band edges, pertaining particularly to the increase in the width of the π-π* states and also the increase in disorder or defect states within the forbidden gap.

5.2.3 *Photoluminescence properties*

Photoluminescence spectra of the p-CN_x:H films deposited as a function of rf power are shown in Figure 5.6. The spectra were deconvoluted using Gaussian fittings as shown in the example in Figure 5.7.

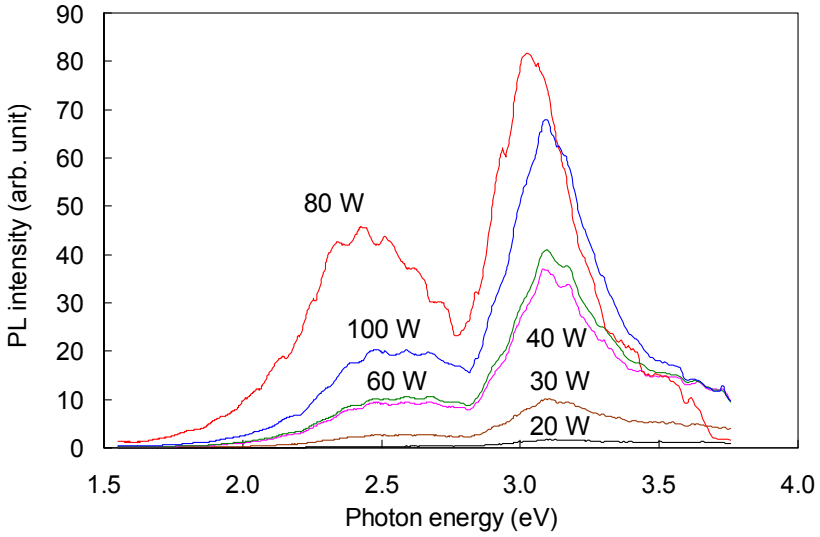

Figure 5.6: Variation in photoluminescence as a function of applied rf power.

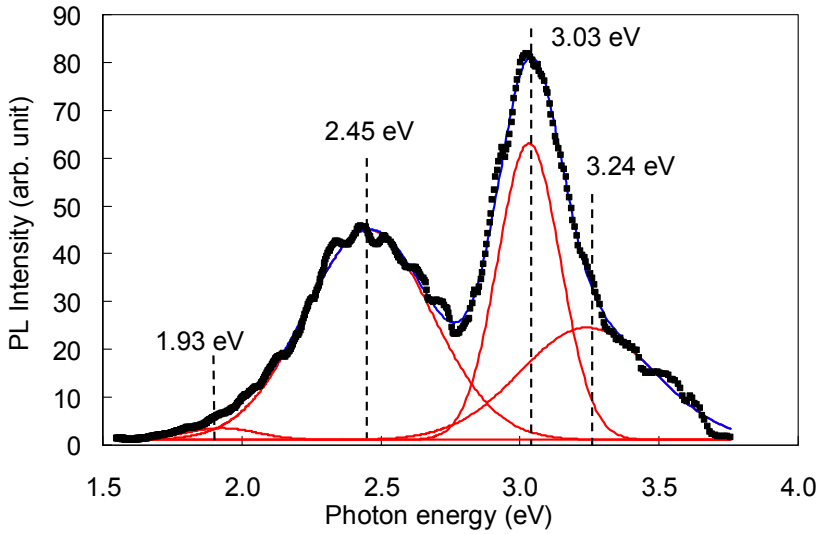

Figure 5.7: Example of photoluminescence Gaussian fitting for the film deposited at applied rf power of 80W.

The fittings show three major peaks at photon energy ranges of 2.48-2.69, 3.03-3.10 and 3.24-3.55 eV. The broad peak in the range of 2.48-2.69 eV is expected to be related to the presence of sp^2 clustering (Daigo and Mutsukura 2004), while the sharp, strong peak at 3.03-3.10 eV is related to the presence of nitrogen bonding in the material (Zhang et al. 1999c). The weaker peak in the range of 3.24-3.55 eV is proposed to originate from the Si substrate background (Zhang et al. 1999c). The variations of the peak intensities and positions at the photon emission range of 2.48-2.69 and 3.03-3.10 eV as a function of rf power are as shown in figure 5.8.

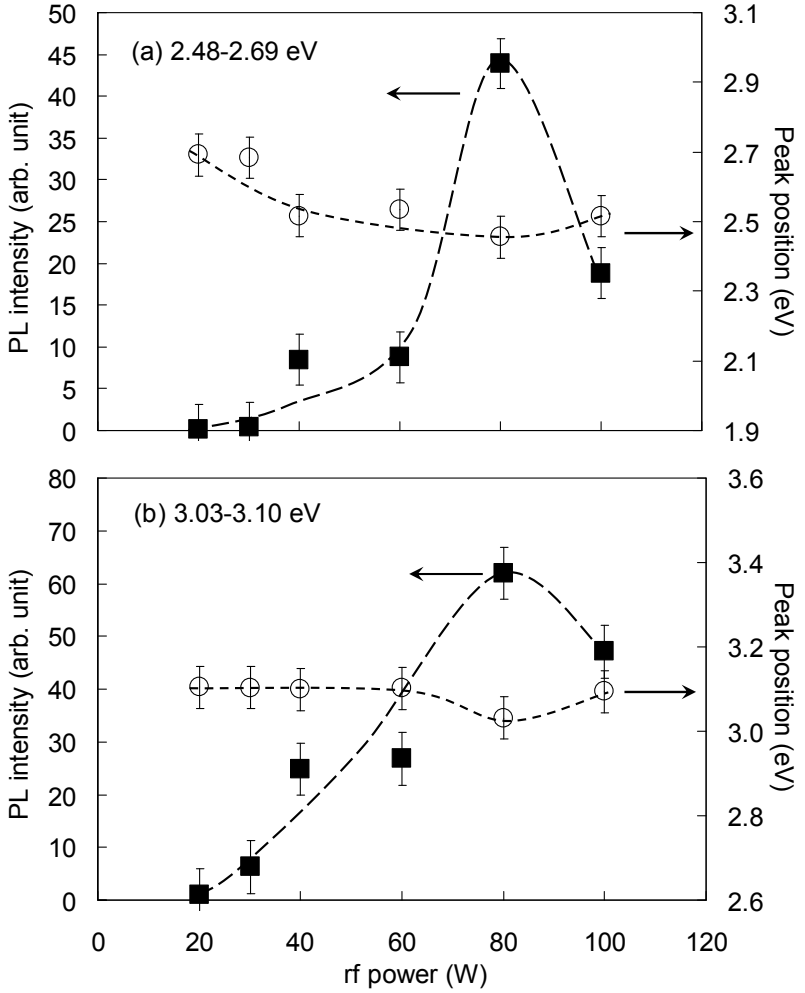

Figure 5.8: Variations of the peak intensities and positions at the photon emission range of (a) 2.48-2.69 and (b) 3.03-3.10 eV for films deposited as a function of applied rf power.

The variations in the peak intensities and positions show two significant aspects. Firstly, it is seen that the PL intensities for both emission energies increase significantly with increase in P_{rf} reaching a maximum for films deposited at P_{rf} of 80W. Above this P_{rf}, the PL intensity deceases. This is in contrast with the report by Mutsukura and Akita (Mutsukura and Akita 2000) which showed a consistent decrease in PL intensity with rf power for their a-CN_x:H films deposited using rf PECVD. However, a similar turn over point in the PL intensity has also been reported by some researchers (Durand-Drouhin et al. 2001; Lejeune et al. 2004) although the critical deposition parameter values differ slightly from this present work. The highest PL intensities at P_{rf} of 80W coincides with a slight decrease in peak position. However, it should be noted that the spectral shape remains the same for all P_{rf} (Figure 5.6) indicating that the origin of the PL in these films remains the same regardless of P_{rf} applied. Similarly, the consistency in the emission energies indicates that the recombination processes remains the same.

The second aspect is seen in the correlation between E_{04} and the PL intensities of these films. This relationship is clearly shown in Figure 5.9 where the PL intensities decrease almost exponentially with E_{04} in the range of 2.95-5.59 eV. This result appears to contradict the reports of various work concerning similar materials (Daigo and Mutsukura 2004; Mutsukura and Akita 2000) which mainly show an increase in PL properties with the increase in optical energy gap. These reports suggest that with the decrease in optical energy gap, which was calculated as the Tauc gap, resulted in a quenching of the PL efficiency due to the increase in non-radiative recombination sites. The contradiction in these findings may be explained by the difference in E_{04} range in question. This is supported by the work of some researchers (Durand-Drouhin et al. 2001; Lejeune et al. 2004) where they have reported a turn over point at a critical E_{04}. This is also seen in this current work, which indicates this critical E_{04} value to be

approximately 2.96 eV for both emission energies. This result also indicates that E_{04} of 2.96 eV and hence the corresponding P_{rf} of 80 W, provides the best condition for radiative recombination to occur where the density of states in these localized centers are at their highest.

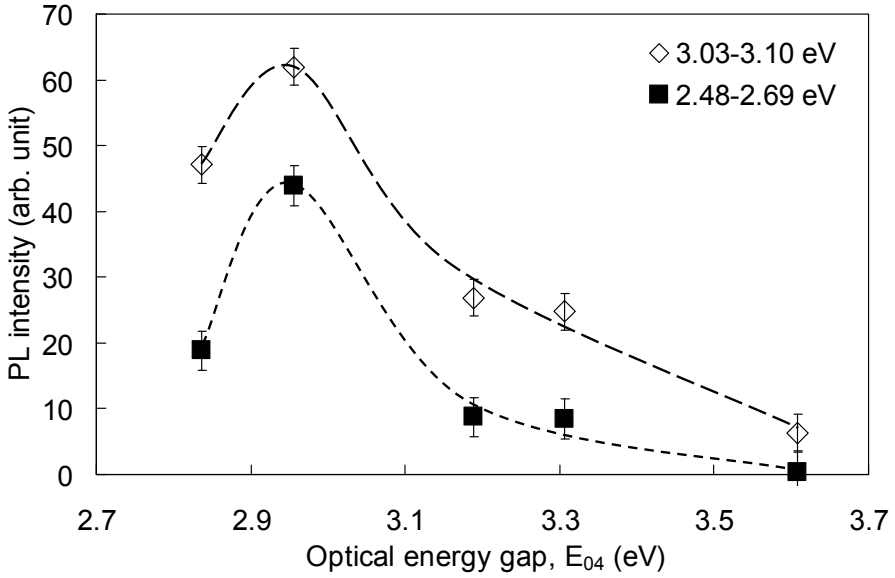

Figure 5.9: Variations of the peak intensities and positions at the photon emission range of (a) 2.48-2.69 and (b) 3.03-3.10 eV for films deposited as a function of applied rf power. Lines are as guide to the eyes.

5.2.4 Elemental composition determined by Auger electron spectroscopy (AES)

The relative nitrogen to carbon ratio of the films were calculated from these spectra and is shown as a function of P_{rf} in Figure 5.10. The N/C remain almost constant within the initial P_{rf} of 20-40 W which may be due to low dissociation of N_2 gas. Subsequently the N/C ratio increases significantly up to a maximum of 0.29 at P_{rf} of 80 W. This may be due to a corresponding increase in N_2 dissociation which increases the secondary reactions in the plasma and thus increases the bonded N in the films. With

further increase in P_{rf} to 100 W, the N/C ratio decreases. Two reasons may contribute to the decrease in N incorporation and both are related to the effects of the high applied P_{rf}. Firstly, there would be a depletion of CH_4 and/or N_2 molecules due to the high dissociation rate and this would decrease the number of CN and N radicals. This in turn would decrease the secondary reactions in the plasma. Secondly with the increase in N^+ ions, there would be an increase in ion bombardment and there would be less inclination for these ions to be imbedded or incorporated into the films.

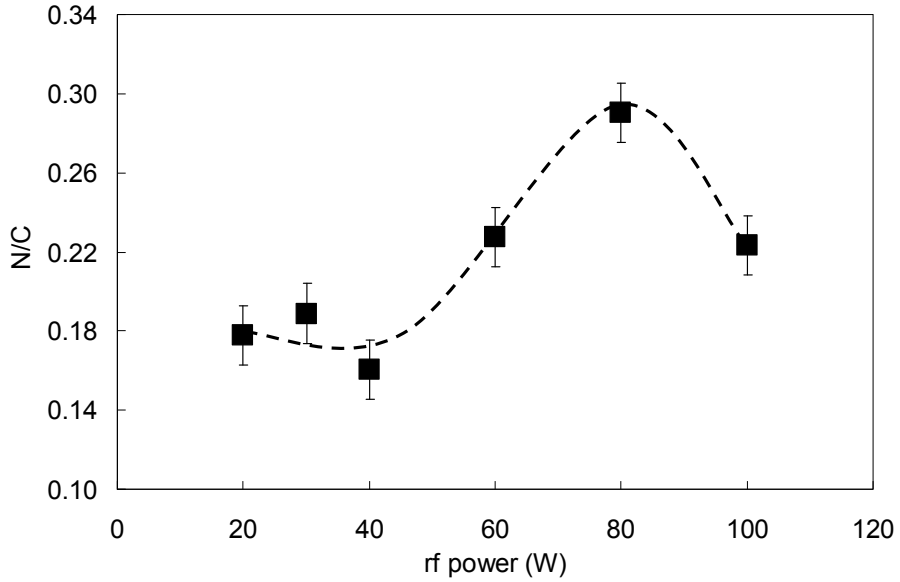

Figure 5.10: Variation of nitrogen to carbon N/C ratio for films deposited as a function of applied rf power.

Another interesting observation in the N/C ratio is the similarity in its variation with that of the PL intensities. This suggest that the relative nitrogen content in the p-CN_x:H films plays a very important role in their PL properties. In view of this, efforts have been made to study the structural and bonding properties of these films and these are discussed in the following sections.

5.2.5 Structural characteristics determined by Raman spectroscopy

The variation in Raman spectra of samples deposited as a function of P_{rf} is shown in Figure 5.11 (a). The spectra clearly show an increase in signal strength as P_{rf} increases which is related to the increase in growth rate, and thus the film thickness with the increase in P_{rf}. The increase in the signal strength also brings about an increase in PL background intensities, where the effect of the PL background increases with the increase in P_{rf}. To further analyze these spectra, the background effects are corrected with a non-linear interpolation and the resulting spectra is deconvoluted using Gaussian line fittings. These fittings are as shown in Figure 5.11 (b). However it is obvious that the Raman signals for film deposited below P_{rf} of 60W are beyond the sensitivity of the instrument utilized. The remaining spectra gave stronger signals from which these Raman parameters were obtained. These are shown in Table 5.2.

Table 5.2: Raman fitting parameter for film deposited as a function of applied rf power.

P_{rf} (W)	N/C	ω_D (cm^{-1})	$FWHM_D$ (cm^{-1})	I_D (a.u.)	ω_G (cm^{-1})	$FWHM_G$ (cm^{-1})	I_G (a.u.)	I_D/I_G
80	0.29	1384 ± 2	143.8	1023.0	1573 ± 1	167.2	974.5	0.95
100	0.22	1360 ± 2	103.9	810.7	1583 ± 2	176.0	1045.8	1.29

The corresponding N/C ratios at these P_{rf} obtained from Figure 5.10 are also included in this table. Raman fitting parameters for P_{rf} of 60W was not included since the intensity of the spectrum was very weak and is almost equivalent to the noise level. This may be due to the relatively lower thickness of the films. According to Neuhaeuser et. al, (Neuhaeuser et al. 2000), certain Raman bands in a-C:N films show significant

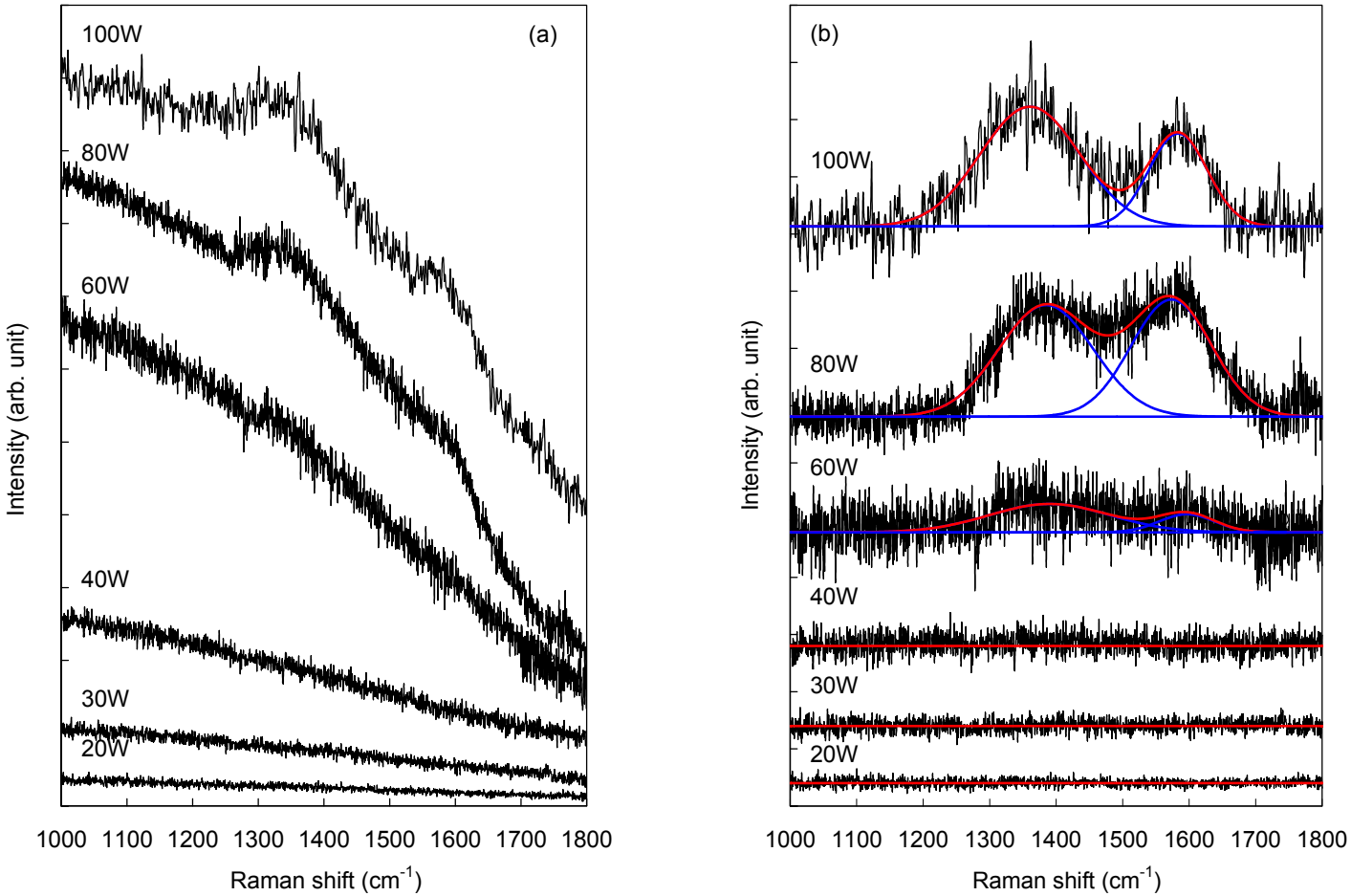

Figure 5.11: Variation in Raman scattering spectra for films deposited as a function of applied rf power, whereby (a) shows the raw data and (b) shows the deconvolution of the Raman spectra after photoluminescence background extraction.

functional dependence on layer thickness, since Raman intensity is directly related to the concentration of active substances. This led to a large fitting error and thus is omitted. Thus, the result of the fitting is only available for films deposited at P_{rf} of 80 and 100W.

Due to the absence of these Raman fittings, it is inappropriate to do any reliable comparative analysis to represent the whole set of films with only these two results. However, it could be concluded from this that for the sake of Raman analysis, with the usage and availability of the current Raman measurement unit, the preferable film for such analysis should come from the choice of either of these two P_{rf}. However in a more remote scale, the Raman fitting for these two spectra does give an indication of the structural difference between the films deposited at P_{rf} of 80 and 100 W.

Table 5.2 showed that ω_G shifts to higher wavenumber when P_{rf} is increased from 80 to 100 W while their N/C value decreases from 0.29 at P_{rf} of 80 W to 0.22 at P_{rf} of 100 W which corresponds to a decrease in nitrogen incorporation. The shift in ω_G towards a lower wavenumber as a result of the increase in nitrogen incorporation has been observed by other researchers (Falkovsky 2008b; Neuhaeuser et al. 2000). They have attributed this to an increase in bond structure disorder and in an increase in sp^3 content. Table 5.2 also showed that I_D/I_G decreases with the increase in N/C ratio. This indicates a decrease in the number and/or size of the graphitic clusters (Cheng et al. 2001b; Ferrari and Robertson 2000). Although this does not authenticate the increase in sp^3 content in the film, it does support the increase in disorder. Additionally, the increase in $FWHM_D$ suggest an increase in disorder due to a distribution of clusters with different order and dimensions (Ferrari and Robertson 2000). These results are in line with the suggestion of the contribution of N incorporation in the film. The sp^2-type

incorporation of nitrogen would generate a significant amount of non-six-fold atomic structures in these films. It is the increase in these structures with the increase in nitrogen incorporation at P_{rf} of 80W that results in the increase in the disorder in the material. In the same way, the decrease in nitrogen incorporation for P_{rf} of 100 W decreases these disorders due to a decrease in non-six-fold atomic structures.

5.2.6 Chemical bonding studies via Fourier transform infrared spectroscopy

FTIR spectra for p-CN_x:H films deposited as a function of P_{rf} is as shown in Figure 5.12.

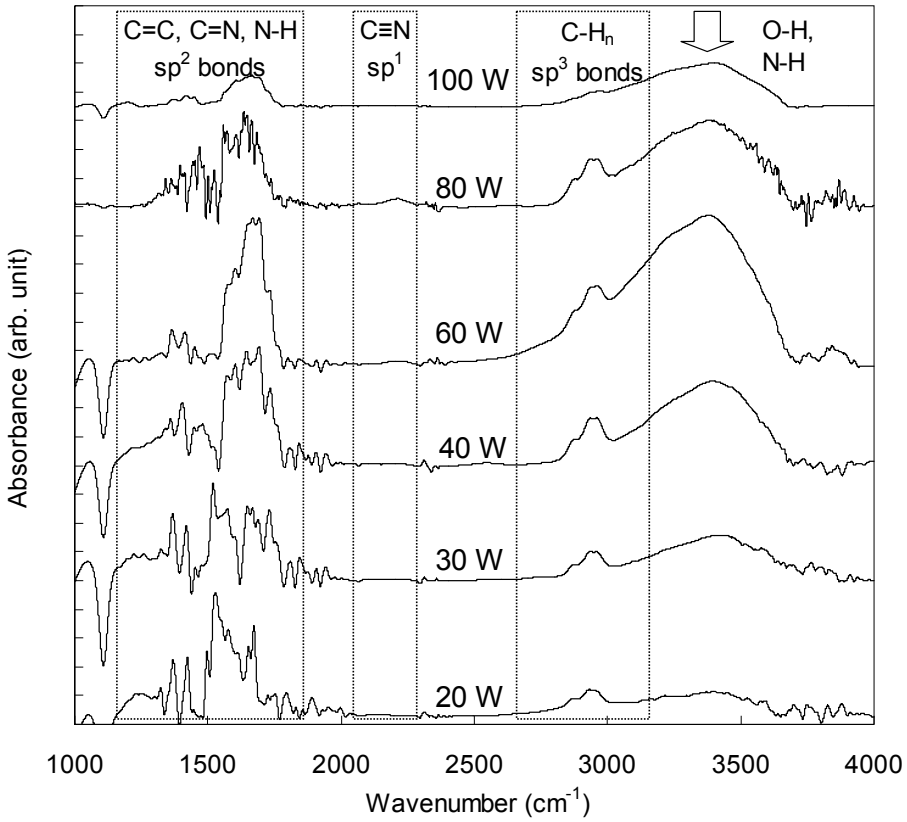

Figure 5.12: Variation in FTIR absorbance spectra for films deposited as a function of applied rf power in the range of 1000-4000 cm^{-1}.

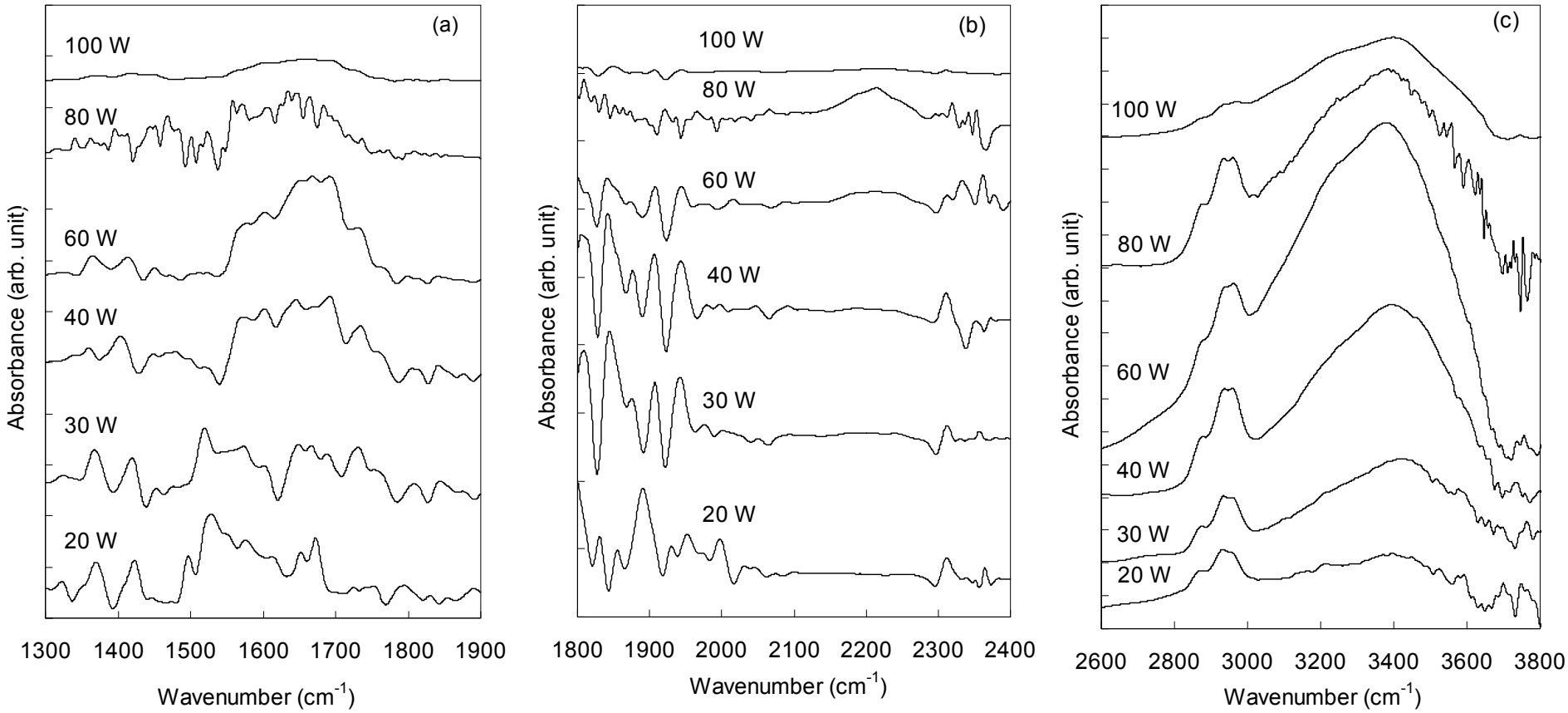

Figure 5.13: Variation in FTIR absorbance spectra for films deposited as a function of applied rf power in the range of (a) sp^2, (b) sp^1 and (c) sp^3 phases.

These spectra could be divided into 3 parts. These include (i) the sp^2 phases comprising, among others, the C=C and/or C=N, and N-H bonds within the wavenumber range of 1300-1900 cm^{-1}, (ii) the sp^1 phase associated with the C≡N groups within the range of 1800–2200 cm^{-1}, and (iii) the groups correlated to the presence of hydrogen comprising of the sp^3 phases of C-H groups within the range of 2800–3000 cm^{-1} and the hydroxyl N-H and/or O-H groups within the range of 3000-3800 cm^{-1} (Motta and Pereyra 2004; Mutsukura and Akita, 2000). For clarification these spectra are shown in individual regions as shown in Figure 5.13.

Figure 5.14 shows the relative intensities of the sp^2 and sp^3 content in the films as a function of P_{rf}, obtained from the integrated intensities of the CH_n groups.

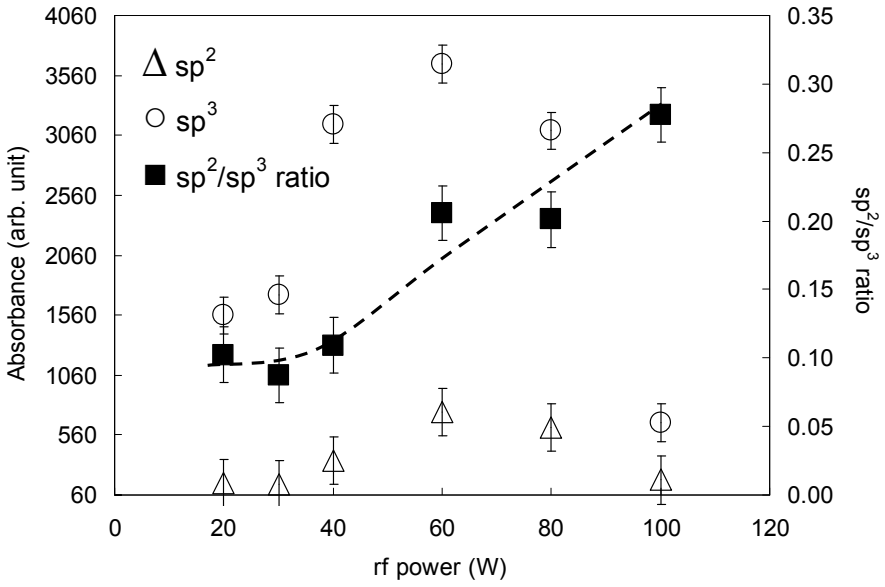

Figure 5.14: Variation in sp^2, sp^3 and sp^2/sp^3 ratio for films deposited as a function of applied rf power.

The increase in the ratio with the increase in P_{rf} explains the decrease in E_{04} for the films seen in Figure 5.5. Indeed the values for the E_{04} are closely related to

broadening of these localized band edges and are dependent on the size and number of sp^2 clusters in the films. Although the nitrogen incorporation into the film may disturb the contribution and relative content of sp^2 C bonds acquired within this region, it was seen from Raman results, that the sp^2 N bonds effectively reduces the graphitic clustering size and/or numbers. Thus the resulting sp^2 N bonds such as C=N, may not contribute significantly to the E_{04} of the films. Indeed as seen in Figure 5.15 (a), the variation corresponding to the C=C and/or C=N bonds does not tally with that of E_{04}, showing that these two parameters may be independent of each other.

On the other hand, the peak corresponding to the C=C, C=N and/or N–H as shown in Figure 5.15 (a) and those of the isonitrile and nitrile peaks shown in Figure 5.15 (b) show similar trend. These peak intensities increase up to a P_{rf} of 60 or 80 W and then decrease with further increase in P_{rf}. The trend in the variation coincides with those of the N/C ratio seen in Figure 5.10, and PL intensities. The similarity to that of the N/C ratio indicates that the peaks, namely the C=N and/or N–H at 1650-1690 cm^{-1} may be due largely to the nitrogen bonds in the films. These results also show the influence on the PL characteristics of the film of the N bonds in the material. The intensities of the isonitrile and nitrile peaks vary differently with the change in applied P_{rf}. From Figure 5.15 (b), while the other bonds show maximum peaks at P_{rf} of 60W, the variation of the peaks at 2215 and 2190 cm^{-1}, corresponding to isolated and/or fused aromatic rings bonded to nitrile (2215 cm^{-1}) and hydrocarbon CH_3 molecules bonded to isonitrile (2190 cm^{-1}) show a maximum peak at P_{rf} of 80 W. These together with the variation in the C=N and/or N–H peaks coincide with the maximum intensity of the film PL intensities.

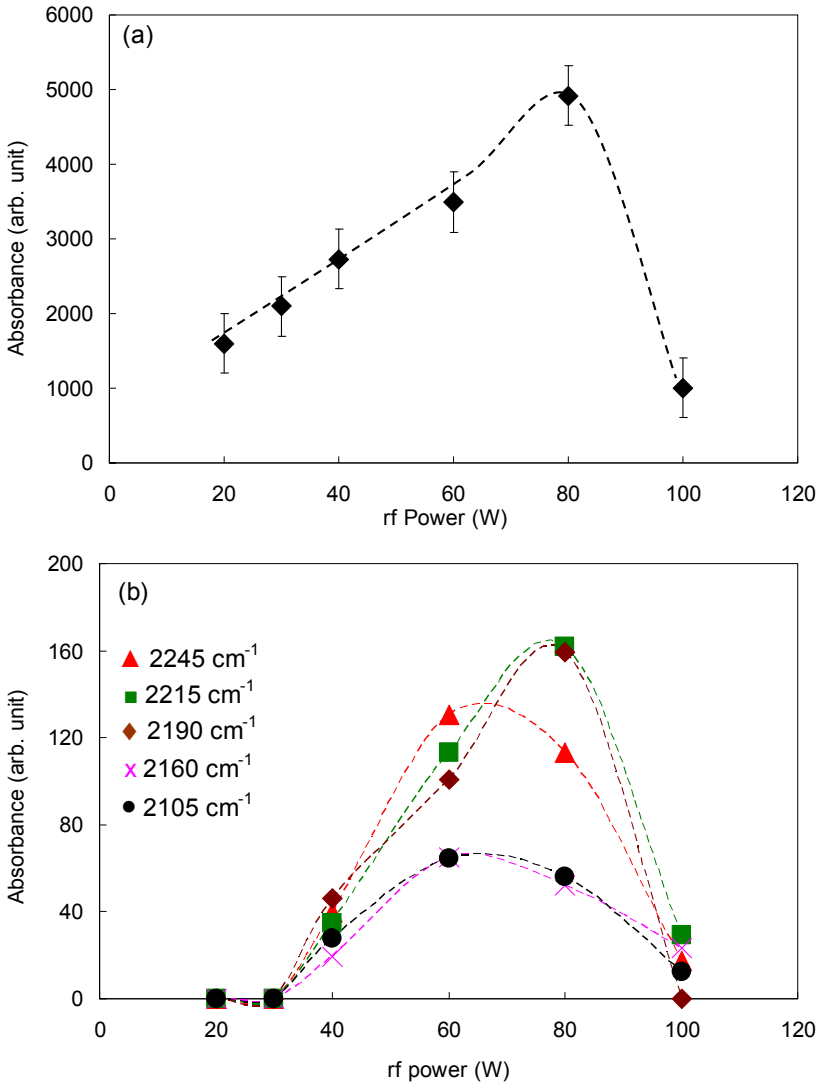

Figure 5.15: Variation in (a) C=C, C=N and/or N–H absorbance peaks and (b) various nitrile and isonitrile absorbance peaks for p-CN_x:H films deposited as a function of applied rf power.

5.3 Effects of Nitrogen-to-Methane Gas Flow-Rate Ratio on the Properties of Polymeric CN_x:H.

Following the studies of P_{rf} on the deposition of these p-CN_x:H films, one parameter which appears detrimental is the nitrogen incorporation. This is studied through the variation of nitrogen-to-methane gas flow-rate ratio, N_2:CH_4. The N_2:CH_4 ratios were calculated as $[N_2/(N_2+CH_4)]$. Examples of available reports indicate a significant influence of the nitrogen incorporation and its content on the structural, optical and bonding properties of the resulting film (Chu and Shiue 2009; Hao et al. 2007; Ito 2008; Messina et al. 2002; Wang et al. 2008a). The progression of the work thus far is depicted in Figure 5.16 and the deposition parameters are shown in Table 5.3 While other parameters were kept constant the N_2:CH_4 ratio was varied from 0.4-0.90. As a reference, films from pure methane (N_2=0) were also deposited.

Table 5.3: Deposition parameters for the study of the effects of nitrogen-to-methane gas flow-rate ratio on the properties of CN_x:H thin films.

	Parameter	Set values
1.	$[N_2/(N_2+CH_4)]$	0, 0.40-0.90
2.	Methane (CH_4) mass flow-rate	20 sccm (fixed)
3.	Nitrogen (N_2) mass flow-rate	varied
4.	rf power	80 W
6.	Electrode distance	5 cm
7.	Initial substrate temperature	100°C
8.	Chamber base pressure	~$1x10^{-5}$ mbar
9.	Deposition pressure	0.8 mbar

*indicates the variable parameter for the study

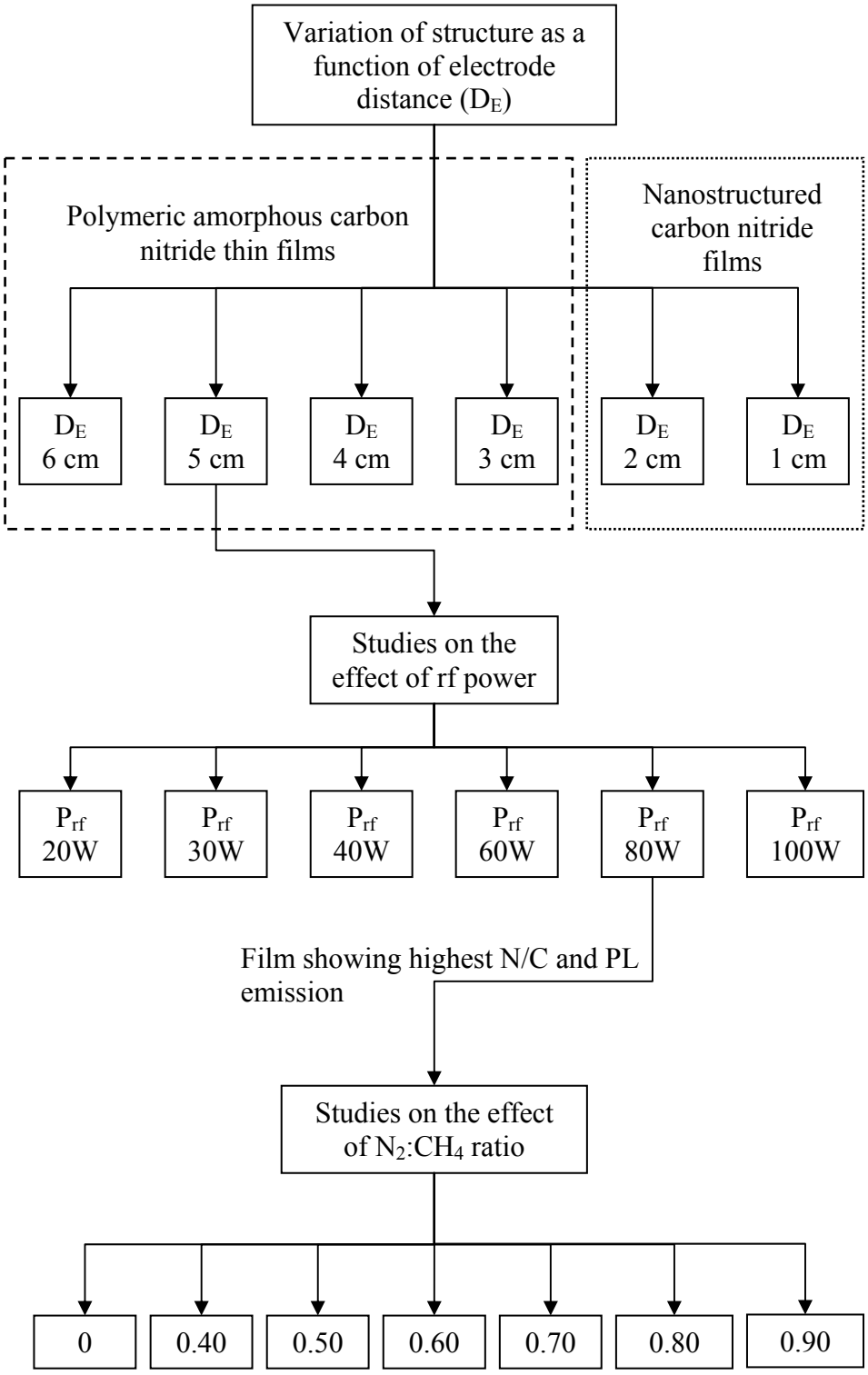

Figure 5.16: Flow chart showing the progression of the current studies of p-CN_x:H films.

5.3.1 Determination of growth rate measured by surface profilometry

Variation in the p-CN_x:H film growth rate as a function of the N_2:CH_4 ratio is shown in Figure 5.17. The growth rate decreases almost linearly with the increase in N_2:CH_4 ratio. This is similar to the report by other researchers (He and Chang 1998; Wang et al. 2008a) and was attributed to a local desorption of nitrogen in the nitrogen-enriched ambient or formation of volatile CN compounds, e.g. C_2N_2 which does not contribute to the growth of the film. This also leads to a decrease in the CH_n radicals in the plasma due to the excess nitrogen (Hao et al. 2007; Motta and Pereyra 2004; Zhou et al. 2006).

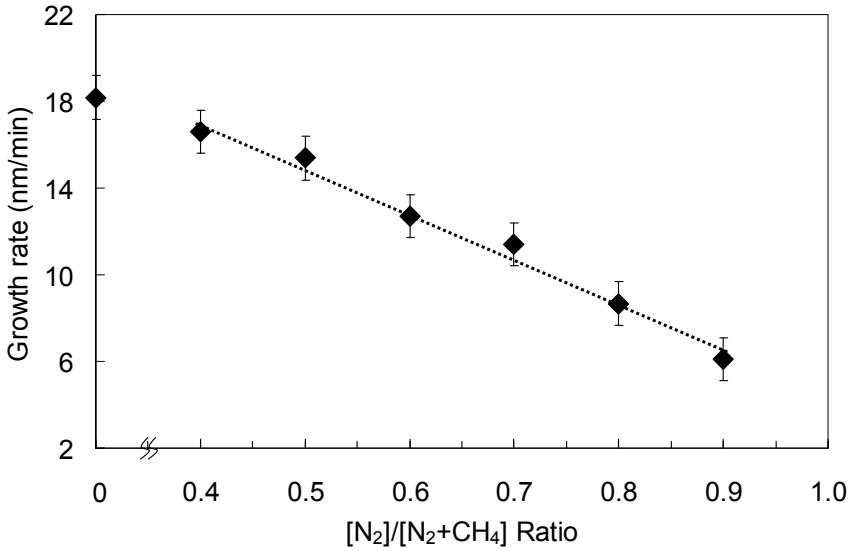

Figure 5.17: Variation of growth rate for p-CN_x:H films deposited as a function of nitrogen-to-methane gas flow-rate ratio. Line is as guide to the eye.

5.3.2 Optical properties measured by UV-Vis NIR spectroscopy

The variations in E_{04} and n of the p-CN_x:H films as a function of N_2:CH_4 ratio are shown in Figure 5.18. The trend in both E_{04} and n are alike where these values decrease gradually to a minimum at a N_2:CH_4 ratio of 0.70, and then increase with

further increase in the ratio. The changes in n are an indication of a structural modification as more nitrogen is introduced into the plasma and incorporated in the film. Similarly the decrease in E_{04} within the N_2:CH_4 ratio range of 0-0.7 is expected to be due to an increase in sp^2 content in the film as more nitrogen bonds are incorporated. The sudden increase in n and more significantly, E_{04} with the increase in the N_2:CH_4 ratio above that of 0-0.7, is quite surprising. Indeed such a trend has not been reported and its contribution to the PL properties of these films is an aspect which is investigated in this work.

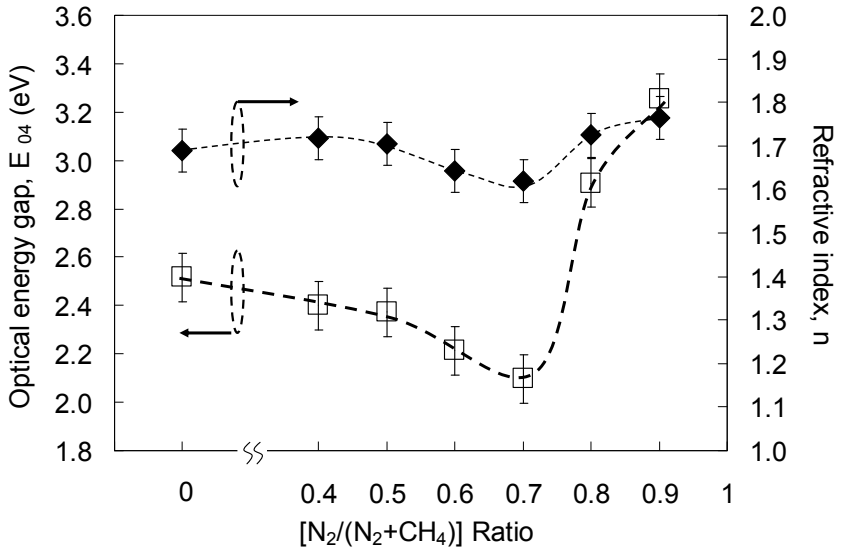

Figure 5.18: Variation of optical energy gap (□) and refractive index (♦) for p-CN_x:H films deposited as a function of nitrogen-to-methane gas flow-rate ratio. Lines are as guide to the eye.

5.3.3 Photoluminescence properties

The variation in PL spectra for p-CN_x:H films deposited as a function of N_2:CH_4 ratio is shown in Figure 5.19. These spectra are similar to those of the films deposited as a function of rf power presented in section 5.2.3. Similar to those, these films showed

Gaussian-fitted peaks within the photon energy ranges of at 2.45-2.56, 3.03-3.10 and 3.24-3.45 eV, which are believed to be attributed to the presence of sp^2 clustering (Daigo and Mutsukura 2004), the presence of nitrogen bonding in the material (Zhang et al. 1999c) and the Si substrate background (Zhang et al. 1999c), respectively. The variations of the peak intensities and positions at the photon emission range of 2.45-2.56 and 3.03-3.10 eV for films deposited as a function of N_2:CH_4 ratio are as shown in Figure 5.20.

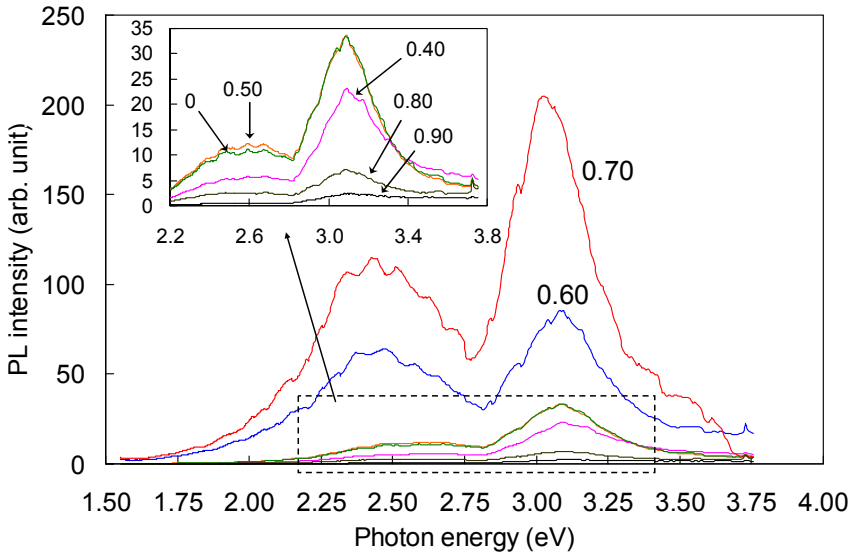

Figure 5.19: Variation in photoluminescence spectra for p-CN_x:H films deposited as a function of nitrogen-to-methane flow-rate ratio. Inset show enlarged selected spectra for ratio of 0, 0.4-0.5 and 0.8-0.9 for further clarification.

The variations in the PL intensities and their peak positions show opposite trends with a significant increase in PL intensities at N_2:CH_4 ratios of 0.60-0.70 coinciding with a decrease in their peak positions. This indicates that the PL intensities are intensified by the narrowing of the radiative recombination centers and that there is a preference in these centers which gives high emission intensities.

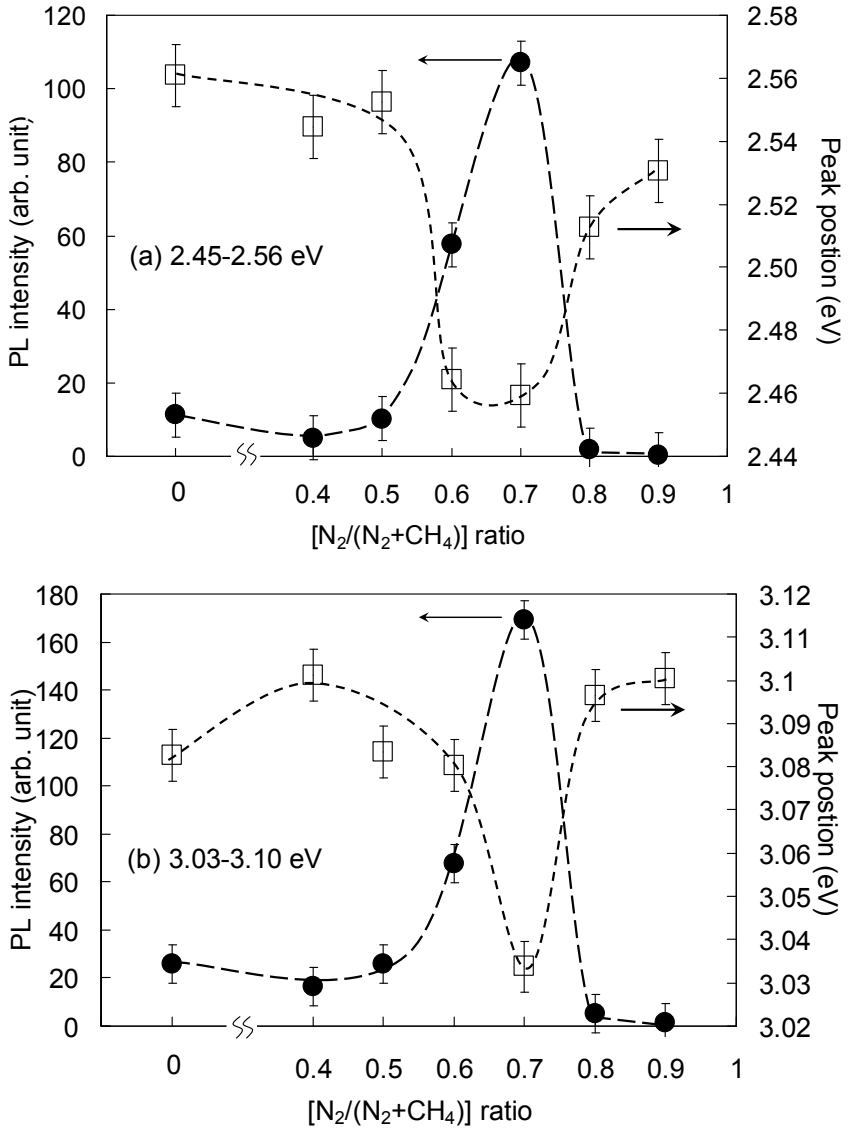

Figure 5.20: Variations of the peak intensities and positions at the photon emission range of (a) 2.45-2.56 and (b) 3.03-3.10 eV for p-CN_x:H films deposited as a function of nitrogen-to-methane flow-rate ratio. Lines are as guide to the eyes.

It is also seen that the variation in the PL intensities and peak positions mirrors that of their E_{04} values. This differs from the trend seen with the change in P_{rf} and could be explained by the contribution of structural changes with the variation in N_2:CH_4 ratio as indicated by their n values. This leads to a significant increase in PL intensities at N_2:CH_4 ratio of 0.70 with a minima in n, E_{04} and the PL peak position.

5.3.4 Elemental composition determined by Auger electron spectroscopy (AES)

The N/C ratio of the films obtained from their AES spectra is shown as a function of N_2:CH_4 ratio in Figure 5.21. The N/C ratio increases with the increase in N_2:CH_4 ratio indicating an increase in N content in the films. It is seen that the variation in the N/C ratio increases almost exponentially up to a N_2:CH_4 ratio of 0.70 and then begins to saturate with further increase in the N_2:CH_4 ratio. The saturation in the N/C ratio is commonly seen for films deposited using rf PECVD (Motta and Pereyra 2004) and even for the carbon nitride films deposited using other deposition methods (Shi et al. 2002). This saturation is one of the major difficulties in obtaining carbon nitride films with high nitrogen content. It is proposed that the saturation in N/C ratio may be due to the preferential formation of volatile CN compounds which removes excess N at a certain degree of N_2 dilution. Nevertheless in this work, the maximum N/C ratio is still significantly high and comparable to the high nitrogen content proposed for theoretical C_3N_4 films (Amir and Kalish 1991; Shi et al. 2002).

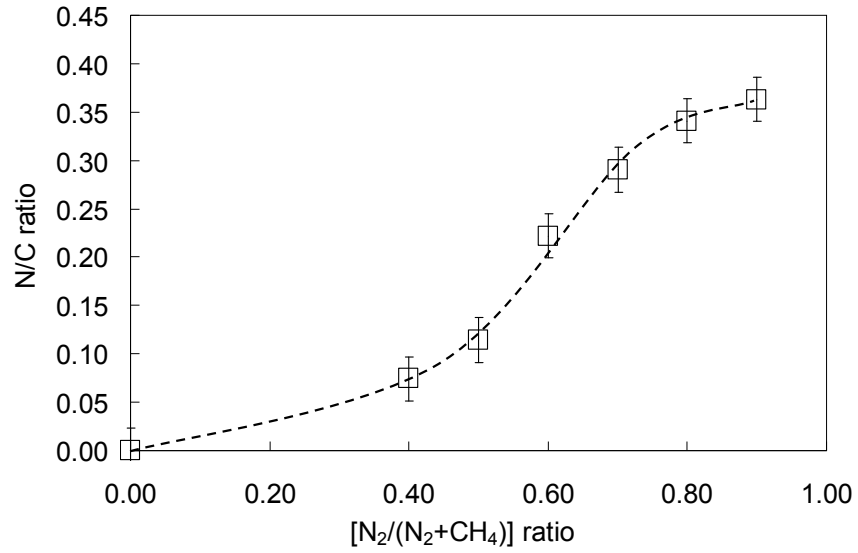

Figure 5.21: Variation of nitrogen to carbon N/C ratio for p-CN_x:H films deposited as a function of nitrogen-to-methane flow-rate ratio. Line is as guide to the eye.

However it is seen that the trend in N/C ratio does not correlate to the trends in the optical characteristics of the films, neither in the E_{04} nor the PL properties. This indicates that the optical characteristics of the films may not only depend on the nitrogen content but also to the way this nitrogen is bonded. This, together with the structural changes indicated by the corresponding change in refractive index of the film may vary the PL intensities of the film with the change in N_2:CH_4 ratio.

5.3.5 Structural characteristics determined by Raman scattering spectroscopy

The structural properties of the films in terms of the sp^2 content are studied using Raman scattering spectra. These spectra are shown in Figure 5.22 (a). The corresponding normalized spectra with baseline correction are shown in Figure 5.22 (b). However it can be seen that apart from the spectrum for the film deposited at a N_2:CH_4 ratio of 0.70, the spectra for the other films show weak peaks at the expected D and G peak positions. The Gaussian fittings for these films are dominated by significant noise levels which effectively increase the error of the fitting parameters. Thus, for this reason comparative analysis of the D and G peak fittings were avoided. On the other hand, in general it is seen that the contribution of the sp^2 content and the resulting clustering is most significant at a N_2:CH_4 ratio of 0.70 indicating that the contribution of the sp^2 bonds in the film is at its highest at this ratio. It is also seen that even at high nitrogen incorporation seen from AES at a N_2:CH_4 ratio of 0.80-0.90, the Raman spectra decreases again which again implies that the type of bonding present in the film with nitrogen incorporation is very important.

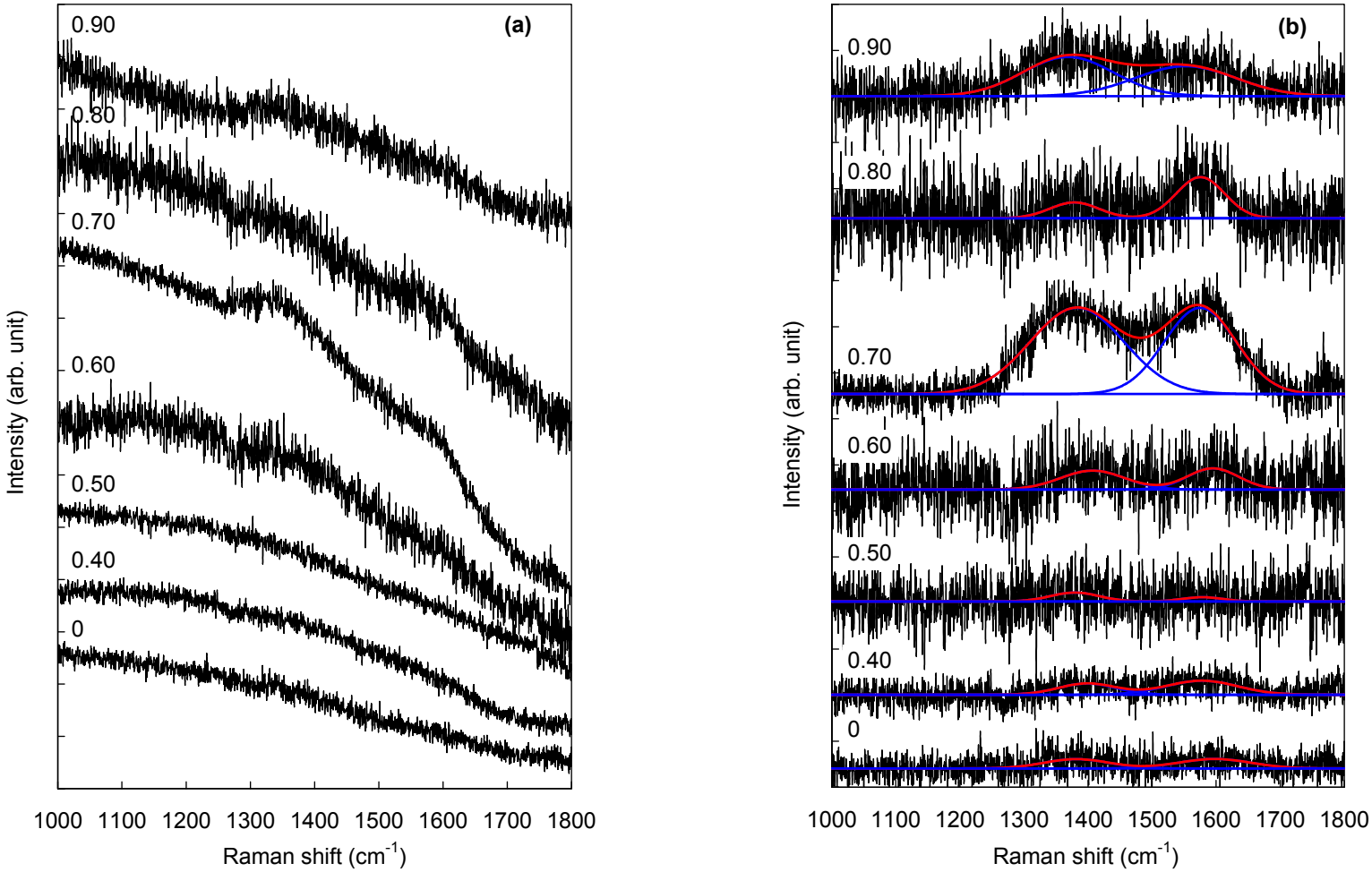

Figure 5.22: Variation in Raman scattering spectra for p-CN_x:H films deposited as a function of nitrogen-to-methane flow-rate ratio, whereby (a) shows the raw data and (b) shows the deconvolution of the Raman spectra after photoluminescence background extraction.

5.3.6 Chemical bonding studies via Fourier transform infrared spectroscopy

The FTIR spectra for the films deposited as a function of N_2:CH_4 ratio are shown in Figure 5.23. The spectra of the films are similar to those previously discussed in section 5.2.6. However there are significant changes in the profile with variation in N_2:CH_4 ratio. These differences are clearly seen in the individual stacking of each spectral region shown in Figure 5.24. These spectra were corrected by eliminating the background contribution using a linear interpolation for each region.

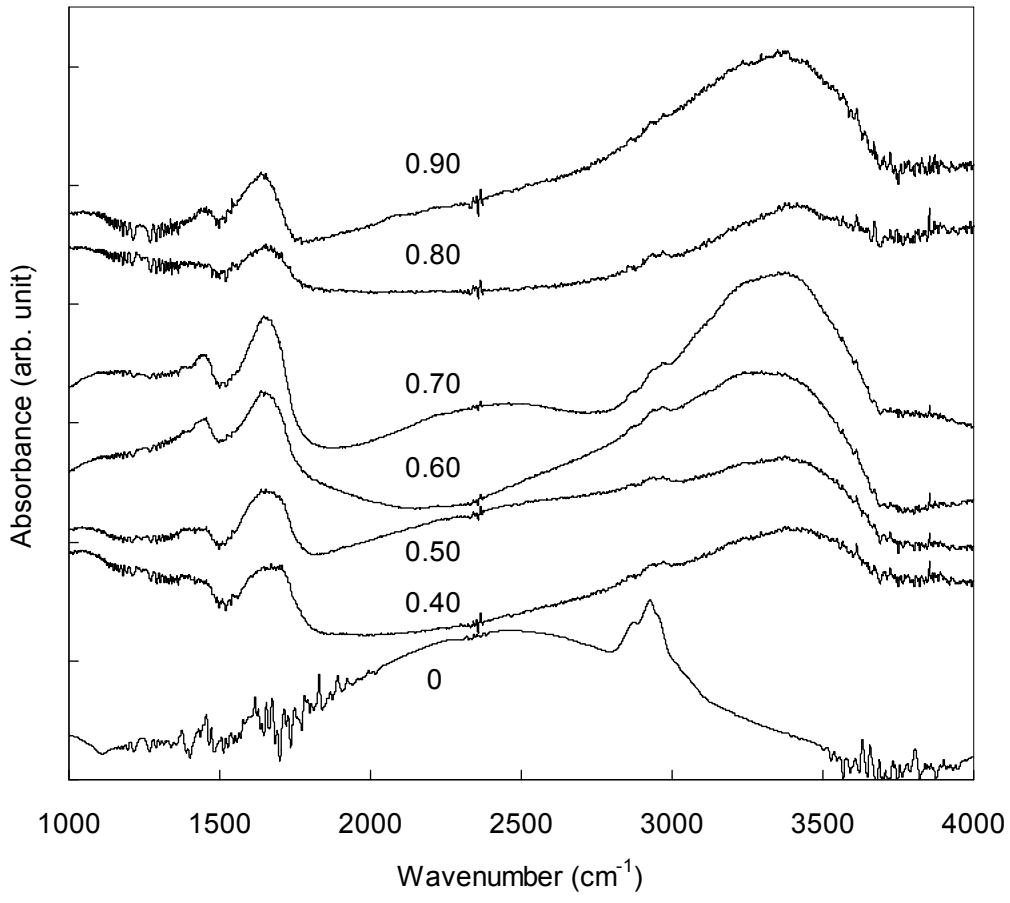

Figure 5.23: Variation in FTIR absorbance spectra for p-CN_x:H films deposited as a function of nitrogen-to-methane flow-rate ratio in the range of 1000-4000 cm^{-1}.

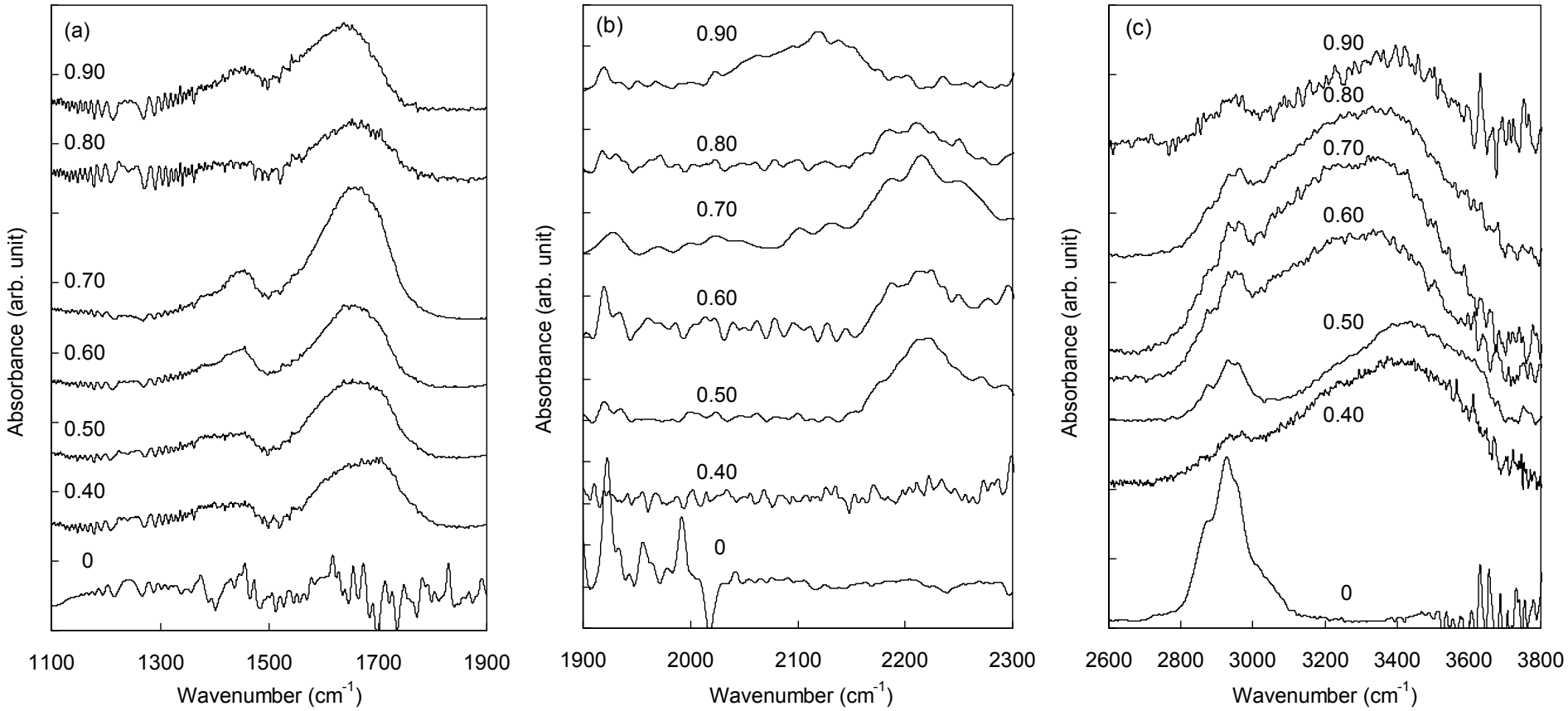

Figure 5.24: Variation in FTIR absorbance spectra for p-CN_x:H films deposited as a function of nitrogen-to-methane flow-rate ratio in the range of (a) sp^2, (b) sp^1 and (c) sp^3 phases.

One of the most significant differences in the spectra is seen in the profile of the film deposited from pure CH_4 without N_2 dilution (N_2:CH_4 ratio of 0). This deposition gives an amorphous hydrogenated carbon, a-C:H film. The FTIR spectrum of this film defers significantly from those with nitrogen gas dilution. The differences shows the effect of nitrogen dilution and incorporation since AES confirms the absence of any nitrogen content in the a-C:H (since nitrogen could have come as contaminant from the sputtering of residues from the chamber). The peak normally associated with the content of sp^2 bonds in the wavelength region of 1300-1800 cm^{-1} (Figure 5.24 (a)) is absent for the a-C:H film. It has been proposed that nitrogen enhances the intensity of the broad band within this range (Rodil and Muhl 2004). This is due to the indirect contribution of nitrogen incorporation which breaks the symmetry of the sp^2 carbon bonds (Kaufman et al. 1989), allowing the band within this region to be IR active. This has been used by many researchers to assume that the bands within this region are associated with the D and G active IR peaks. However, the results in this work, both from the variation in rf power and N_2:CH_4 ratio, supports Rodil and Muhl (Rodil and Muhl 2004) in this matter. The variation in the D and G peaks (shown in Appendix 2) assumed from the IR spectra does not agree with the Raman results particularly on the profile and values of the D/G ratio for the film deposited at N_2:CH_4 ratio of 0.70. Also no correlation between these results and the other properties such as E_{04}, was found.

Additionally, the peaks at the wavenumber range of 1900-2300 cm^{-1} which could also originate from the C≡C bonds in the material is absent for that of the a-C:H film. This suggests the fact that the peaks found within this range for the nitrogenated films are due to the nitrogen bonds in the films, namely those of nitrile and isonitrile bonds. Similarly, the broad peak within the wavenumber range of 3100-3700 cm^{-1} normally associated with O-H and/or N-H is also absent in the a-C:H film. The only

clearly identifiable peaks for the a-C:H film are those associated with the CH_n bonds within the wavenumber range of 2700-3100 cm^{-1}. These are prominent peaks compared to the nitrogenated films and indicates the significance and dominance of C-H bonds in the a-C:H film.

For the p-CN_x:H films, the most significant changes are seen in the wavenumber range of 1500-1800 cm^{-1} and the nitrile/isonitrile groups at 2000-2300 cm^{-1} as seen in Figure 5.24 (a) and 5.25 (b), respectively. These peaks are related to the variation in the nitrogen bonds in the films. The changes within the wavenumber range of 1500-1800 cm^{-1} is shown in Figure 5.25 which also shows the relevant Gaussian fittings. There is an apparent decrease in the shoulder peak at approximately (1702 ± 9) cm^{-1} which is believed to be the peak corresponding to N-H bonds in the films (Zhang et al. 2000). Furthermore, the spectra show that at N_2:CH_4 ratios above 0.70, the peak corresponding to the N-H bonds disappears leaving a single peak. The spectra also indicate that as the N_2:CH_4 ratio increases, the C=C and/or C=N bonds in the film identified as the peak centered at (1636 ± 10) cm^{-1} becomes more dominant than that of N-H. This suggests that C=N is the preferential bonding configuration of N in the films with an increase in nitrogen incorporation (seen from N/C ratio from AES). Here N seems to prefer to be bonded doubly with C rather than being bonded to H within the C network. This may explain the decrease in the O-H and/or N-H peak intensities observed at 3100-3800 cm^{-1} as shown in Figure 5.24 (c).

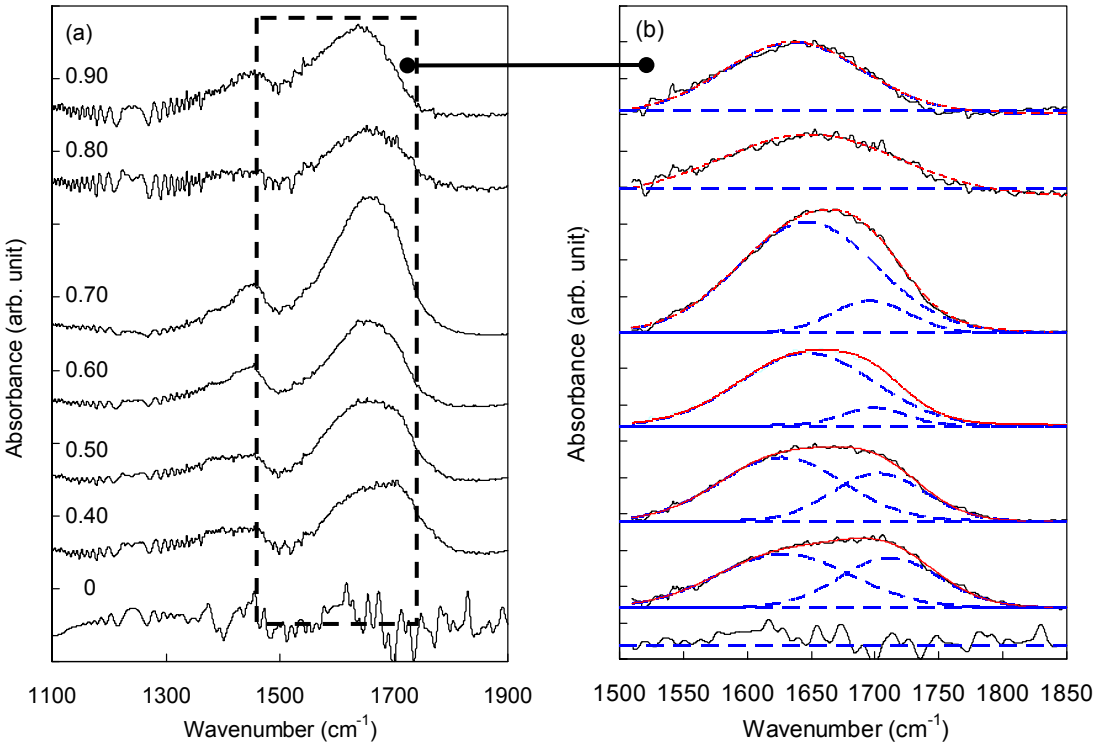

Figure 5.25: FTIR spectra in the region of 1100-1900 cm^{-1} showing the variation in the N-H, C=C and/or C=N bonds for p-CN_x:H films deposited as a function of nitrogen-to-methane flow-rate ratio.

The variation in the C=C and/or C=N bonds with the changes in N_2:CH_4 ratio is shown in Figure 5.26 (a). The peak intensities increase progressively with increase in N_2:CH_4 ratio up 0.70. With further increase in N_2:CH_4 ratio above this point, the ratio decreases. There appear to be some correlation in the variation in this peak and that of the PL intensities. In particular the film at a N_2:CH_4 ratio of 0.70 has the highest PL intensity and also shows the highest C=C and/or C=N bonds content. However the quenching of the PL intensities above this ratio is not dependent only on these bond intensities since the absorption of the peaks of these films is still significantly high.

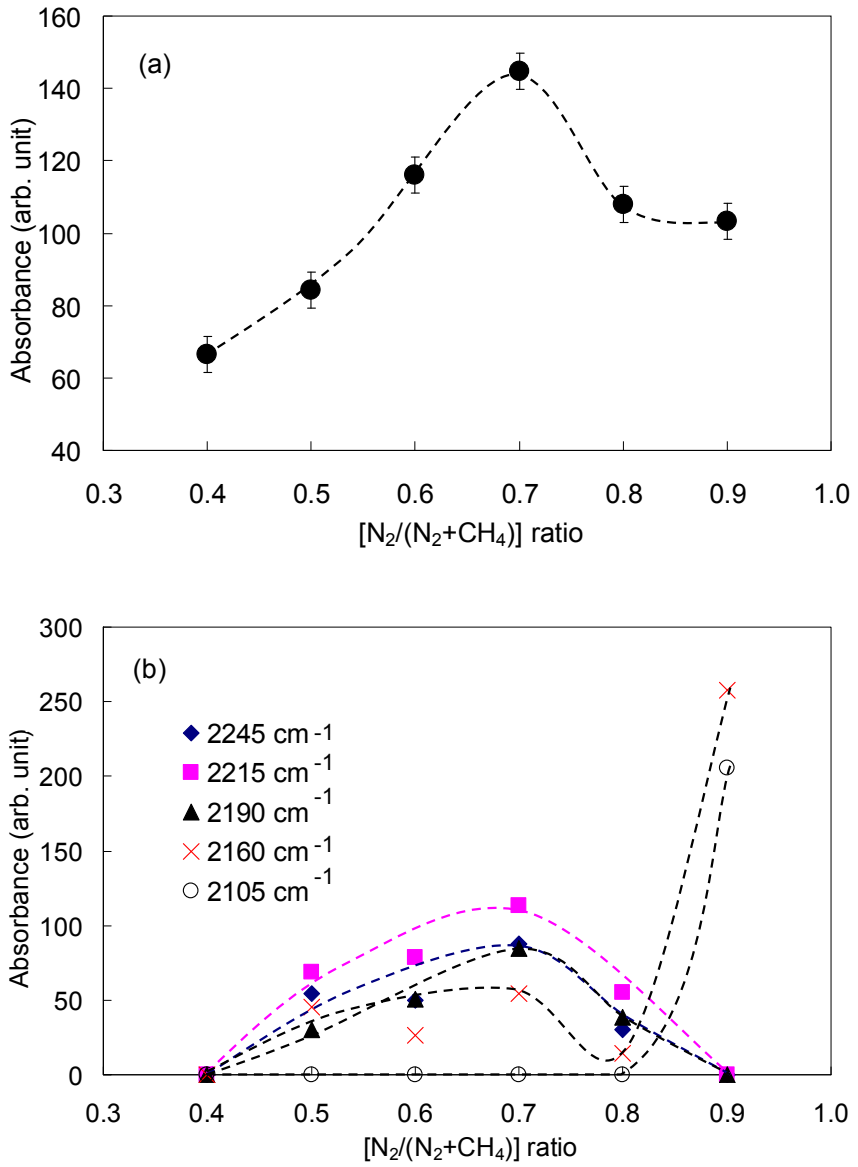

Figure 5.26: Variation in (a) C=C and/or C=N and (b) various nitrile and isonitrile absorbance peaks for p-CN_x:H films deposited as a function of nitrogen-to-methane flow-rate ratio. Line is as guide to the eye.

On the other hand, it is seen that the variation in the isonitrile and nitrile peaks shows a closer relationship with the PL intensities and PL peak position. The FTIR spectra in the wavenumber range of 2000-2300 cm^{-1} were deconvoluted using Gaussian fittings for five peaks associated with the isolated and/or fused aromatic rings bonded either to isonitrile (−N≡C) at 2105 cm^{-1} or nitrile (−C≡N) at 2215 cm^{-1} and hydrocarbon

molecules which include C_2H_5 at 2160 cm^{-1} and CH_3 at 2190 cm^{-1} bonded to isonitrile (−N≡C) and the hydrocarbon groups (CH_3, C_2H_5, etc.) bonded to nitrile (−C≡N) located as a single peak at 2245 cm^{-1} (Mutsukura and Akita 2000; Mutsukura and Daigo 2003). The variation in these peaks as a function of N_2:CH_4 ratio is shown in Figure 5.26 (b). In the initial increase in N_2:CH_4 ratio, all but the peak at 2105 cm^{-1} increase to reach a maximum at the ratio of 0.70. With further increase in the ratio from 0.80-0.90 the peaks at 2190, 2215 and 2245 cm^{-1} decrease and finally disappear at a N_2:CH_4 ratio of 0.90. In contrast, both peaks at 2105 and 2160 cm^{-1} increase significantly at a N_2:CH_4 ratio of 0.90 with the disappearance of these three peaks.

The profile of these five peaks may explain the PL properties of the film and may give an indication of the recombination centers associated with its PL emission. It is noted, however, that the C≡N bonds in the material are not the only factor which determines the recombination centers in these films. There are numerous reports that show its non-nitrogenated and even nitrogenated carbon counterparts (with different or similar structures) show strong PL properties, which were normally attributed to the π-π* emission within the sp^2 C clusters in the films. Nevertheless, the correlation of the C≡N bonds in the film is supported by the works of Mutsukura (Mutsukura and Akita 1999a, 1999b, 2000; Mutsukura 2001; Mutsukura and Daigo 2003). Even in this work such a strong correlation could not be ignored. The contribution and relationship between the C≡N bonds and the sp^2 clustering in term of their correlation with the PL properties could be explained by the presence of lone pairs contributed by the sp^1-C from the C≡N bonds. As discussed in section 4.3.5, these lone pairs could interact with the molecular π orbital formed by neighbouring clustered C and/or N atoms (Fanchini et al. 2002a). This would lead to a modification in the π-π* transition due to the effects of "orbital mixing" and result in an appearance of a broadening of the π band of the film

due to a broadening of the density of states. Indeed this is supported by the decrease in the optical energy gap, E_{04} (Figure 5.18) where E_{04} is inversely proportional to the width of the π band of the film.

Coming back to the variation in these five bands, the bands related to those of the 2190, 2215 and 2245 cm^{-1} peak position mirrors the variation in both E_{04} and PL intensities. However, as seen in section 5.2.6 and the corresponding Figure 5.15, the peak pertaining to the position at 2245 cm^{-1} could be eliminated since its contribution to the E_{04} and PL was found to be insignificant. Thus, the observations in section 5.2.6 and the results in this section agree that the peaks at 2190 and 2215 cm^{-1} are the most probable lone pair contributors and may also act as radiative recombination centers. This may explain the decrease in the photon energy at the highest PL intensity which coincides with the decrease in E_{04}. As mentioned, the band at 2190 cm^{-1} is attributed to CH_3 bonded to isonitrile, while that of 2215 cm^{-1} is attributed to isolated and/or fused aromatic rings bonded to nitrile (−C≡N). These two bands are vastly different and at the current moment the significance of their bonding configuration and how they contribute to the properties of the film PL and E_{04} characteristics are not fully understood.

5.4 Effects of Thermal Annealing on the Properties of Polymeric CN_x:H.

Thermal annealing presents an effective method to study the properties of these p-CN_x:H. With reference to studies done by other researchers, the objective of thermal annealing usually involves the modification in (i) structure and composition (Huang et al. 2007b; Lejeune and Benlahsen 2008; Li et al. 2003b; Zhou et al. 2003), (ii) optical properties (Adhikari et al. 2008; Bouzerar et al. 2005; Zhang et al. 2000) and (iii) PL characteristics (Conway et al. 2000; Mutsukura 2001). In general, these studies allowed the determination of thermal stability and also reveal other aspects which were not apparent in the previous studies on the effect of rf power and N_2:CH_4 ratio.

Efforts to correlate the structural changes and optical characteristics (including E_{04} and PL) were undertaken. For this reason, and also due to the limited availability of some of the characterization equipments, these studies were carried out beginning with FTIR analysis, profilometry and UV Vis NIR spectroscopy. These measurements were done at lower annealing temperature, T_A increment. From the changes seen in the analytical results of these measurements (FTIR in particular), cut sections of the film were annealed at selected temperatures and subsequently were measured using AES, Raman scattering and PL. Thus, although the latter may show fewer data points, any changes seen are strongly supported by the former. The film chosen for this annealing study was selected according to the optimized parameters; both from the studies of rf power and N_2:CH_4 ratio. The criteria for the selection were based on the highest N incorporation, strongest Raman scattering signal and highest PL emission. The progression of the work up to this point is shown in Figure 5.27.

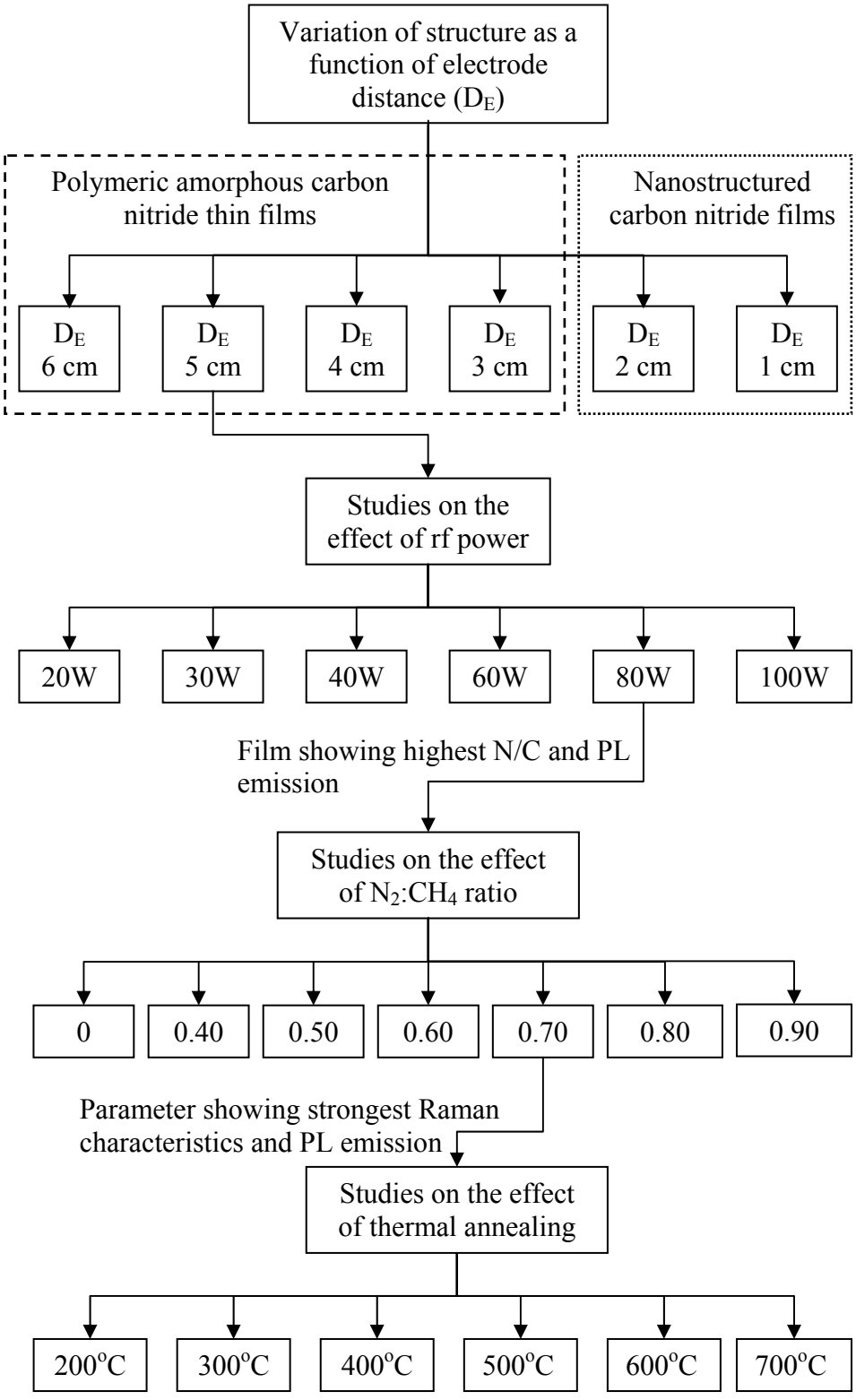

Figure 5.27: Flow chart showing the progression of the current studies of p-CN_x:H films.

5.4.1 Thickness variation measured by surface profilometry

The variation in p-CN_x:H film thickness as a function of annealing temperature is shown in Figure 5.28. The film thickness begins to change only above an annealing temperature, T_A of 200^{o}C. Within the T_A range of 200 – 700 ^{o}C, the film thickness decreases almost linearly with increase in T_A. The decrease in the film thickness has been observed by other researches (Bouzerar et al. 2005; Kulisch et al. 2000). Their studies have shown that the decreasing thickness is due to the combination of densification and/or structural rearrangement within the films. Thus, the decrease in these film thicknesses suggests a change in the film structure with the increase in T_A.

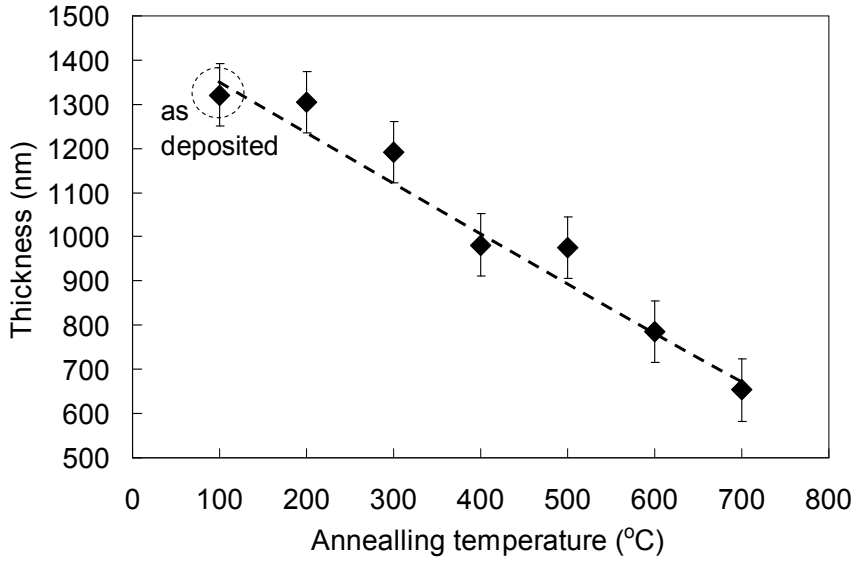

Figure 5.28: Variation of film thickness as a function of annealing temperature. Line is as guide to the eye.

5.4.2 Chemical bonding studies via Fourier transform infrared spectroscopy

FTIR spectra of the p-CN_x:H films annealed at different T_A is shown in Figure 5.29.

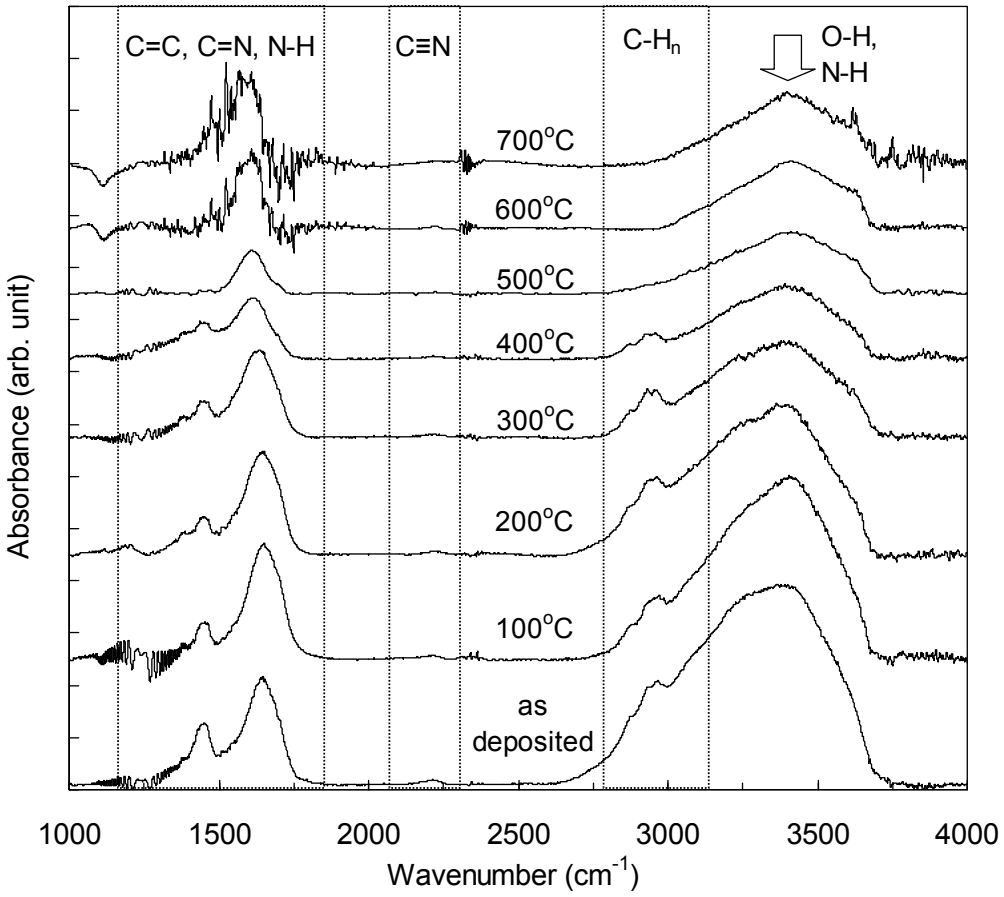

Figure 5.29: Variation in FTIR absorbance spectra as a function of annealing temperature in the range of 1000-4000 cm^{-1}.

For further clarification and assessment of the spectra, the compiled spectra for each range and corresponding functional growth are segregated into individual graphs. These graphs are shown in Figure 5.30. Figure 5.30 (b) and (c) were used to assess the contribution of sp^1 C≡N and hydrocarbon CH_n, respectively, while from Figure 5.30 (a) both the contribution of sp^2 C=C (or/and C=N) and N-H were studied. These spectra

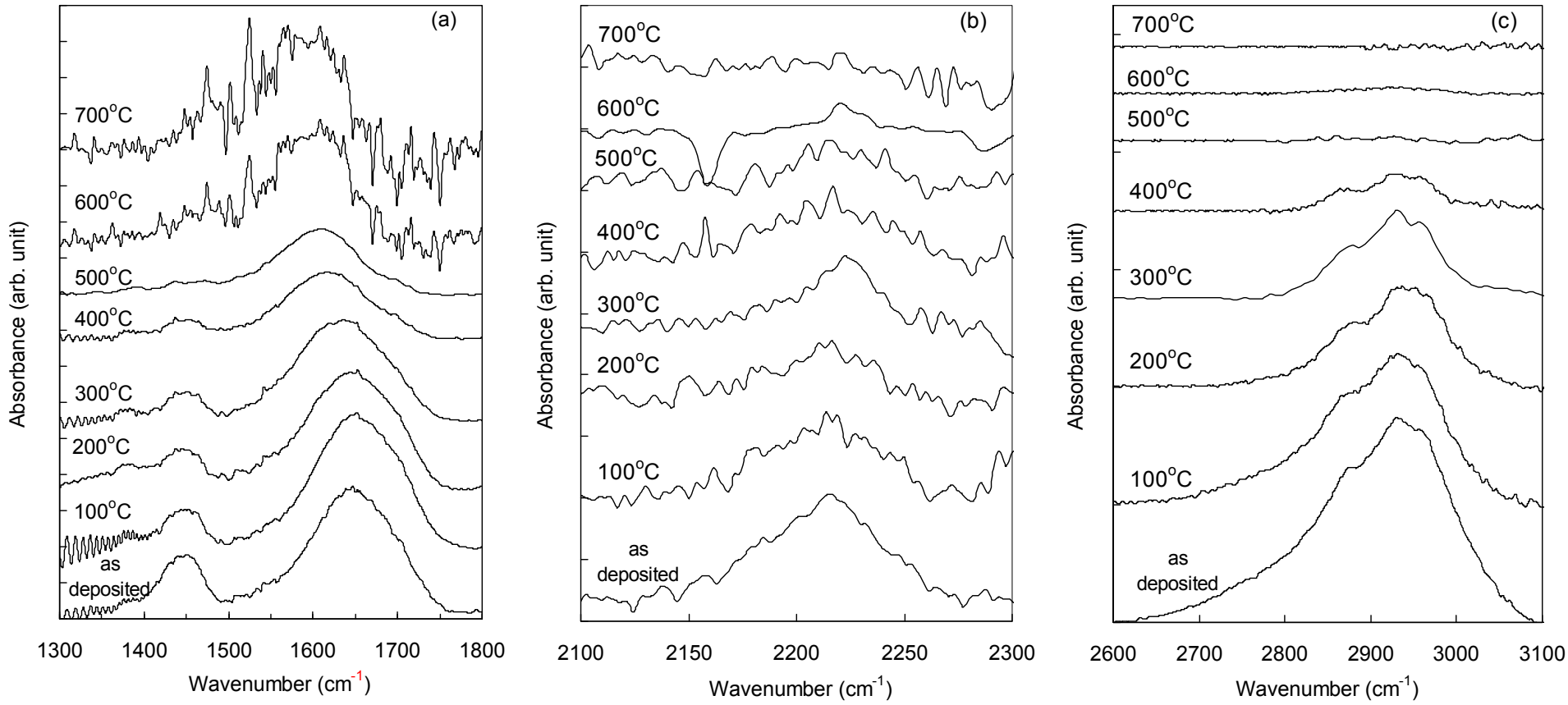

Figure 5.30: Variation in FTIR absorbance spectra as a function of annealing temperature in the range of (a) sp^2, (b) sp^1 and (c) sp^3 phases.

were normalized and baseline corrections were carried out by using standard non-linear fittings. Additionally, the spectra for the CH_n functional groups were corrected by removing the OH and/or NH contribution using Gaussian fittings. The OH and/or NH bonds appear to be present after each annealing cycle which suggests that these bonds are associated with post-contaminants due to the absorption of OH when these samples are exposed to air. A decrease in the shoulder peak at approximately (3250 ± 5) cm^{-1} with increase in T_A suggests that this peak originates from N-H which is similar to that suggested by Zhang et al. (Zhang et al. 2000). This also indicates that the corresponding dominant peak centered at (3410 ± 5) cm^{-1} could be ascribed to that of OH bonds. Additionally, it is seen that the peaks corresponding to the N-H, C=N, C≡N and CH_n groups decrease monotonically with increase in T_A. For clearer assessment of these functional groups, the spectra within each range were deconvoluted and the variations of the main peaks were analyzed. These variations are shown in Figure 5.31.

The variation in the various functional groups depicted in Figure 5.31 could be summarized as follows:

(i) in general the intensity of the signal from the bonds, except for C=C and/or C=N, decrease monotonically with increase in T_A and totally dissociate above the critical T_A of either 500 ^oC or 700 ^oC.

(ii) CH_n groups for both sp^2 and sp^3 configurations disappear at 500 ^oC and can be attributed to the dissociation of H from the CH bonds.

(iii) nitrogen bonds in the films are relatively stable compared to H bonds. The nitrile bonded to fused and/or isolated aromatics are seen as a band centred at approximately (2217 ± 6) cm^{-1} and isonitrile bonded to CH_3 dissociated at T_A of 500 ^oC. On the other hand, the nitrile peak at (2240 ± 11) cm^{-1} and isonitrile at

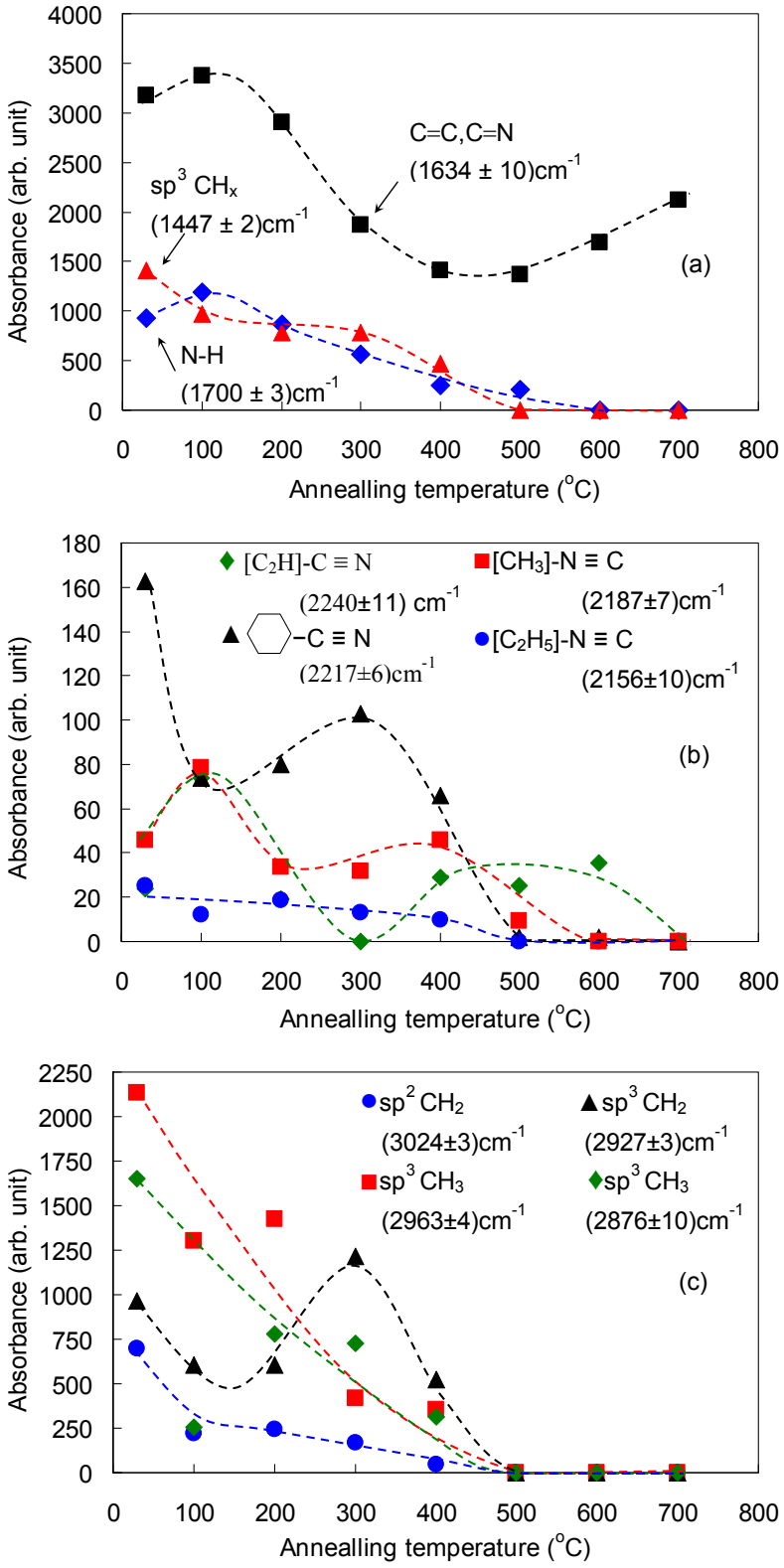

Figure 5.31: Variation in absorbance intensities of various FTIR deconvoluted peaks including (a) C=C and/or C=N, sp^3 CH_x and N-H, (b) various nitrile and isonitrile bonds, and (c) various CH_n bonds for p-CN_x:H films as a function of annealing temperature. Lines are as guide to the eye.

(2156 ± 10) cm^{-1} remain up to T_A of 700 ^oC and 600 ^oC, respectively. The result also shows that N-sp^3 C bonds have higher thermal stability that N-sp^2 C bands, similar to the observations by other researchers (Li et al. 2003c)

(iv) It is seen that the C=C and/or C=N bonds in the films decrease with T_A up to 500 ^oC and then increase significantly with further increase in T_A.

The initial decrease in the C=C and/or C=N peak intensities and hence their content up to T_A of 500 ^oC coincides with the decrease in N bonding in the film. This suggests that the initial decrease in the absorption intensity may be attributed to the decrease in C=N bonds in the films. Indeed, Figure 5.30 (a) shows a decrease in the shoulder peak at approximately 1700 cm^{-1} with increase in T_A. This peak is associated with the N-H bonds (Zhang et al. 2000). Similarly the peak corresponding to sp^3 CH bonds centered at approximately (1450 ± 5) cm^{-1} decreases gradually with increase in T_A. The peak position of the sp^2 C=C or/and C=N bonds shifts from approximately (1650 ± 2) cm^{-1} to lower wavenumber with decrease in the N-H and sp^3 CH bonds. With the disappearance of the N and H bonded peaks, the peak position of the sp^2 C=C or/and C=N bonds becomes constant at (1603± 5) cm^{-1}. It is said that C=N peaks would appear within the wavenumber range of 1620-1670 (Kulisch et al. 2000). These are non-aromatic sp^2 bonds which are interpreted as linear aliphatic CN_x components. Whereas, the peak ascribed to C=C is found at a lower wavenumber around 1600 cm^{-1}(Gharbi et al. 2008) and the bonds are related to the presence of aromatic components in the film. The decrease in this peak position from approximately 1650 cm^{-1} to 1603 cm^{-1} is attributed to the loss of N which decreases the C=N content and thus increases the C=C through reconnection of the severed bonds. Indeed the higher wavenumber prescribed to the as-deposited films (and for T_A below 500 ^oC) is due to the higher electronegativity of nitrogen as compared to carbon (Gharbi et al. 2008) resulting in the higher bonding

energy of C=N. Thus, the increase in the C=C content increases the peak intensity, as shown in Figure 5.31 (a). This coincides with the removal of H and some of the N bonds in the material at this critical T_A value, which leaves dangling bonds that could reconnect to form these C=C bonds in the films (Zhang et al. 2000). With the total dissociation of the CH_n bonds at 500 ^oC and progressive removal of C≡N bonds at and above this temperature, the formation of C=C bonds is promoted and its content is increased. The increase in C=C bonds is in line with graphitization of the film and indicates that with an increase in T_A particularly above 500 ^oC, the structure of the film changes from a polymeric to a more graphitic-like nature.

5.4.3 Optical properties measured by UV-Vis NIR spectroscopy

From the optical spectra, the optical energy gap E_{04}, as a function of annealing temperature was studied. This variation is shown in Figure 5.32.

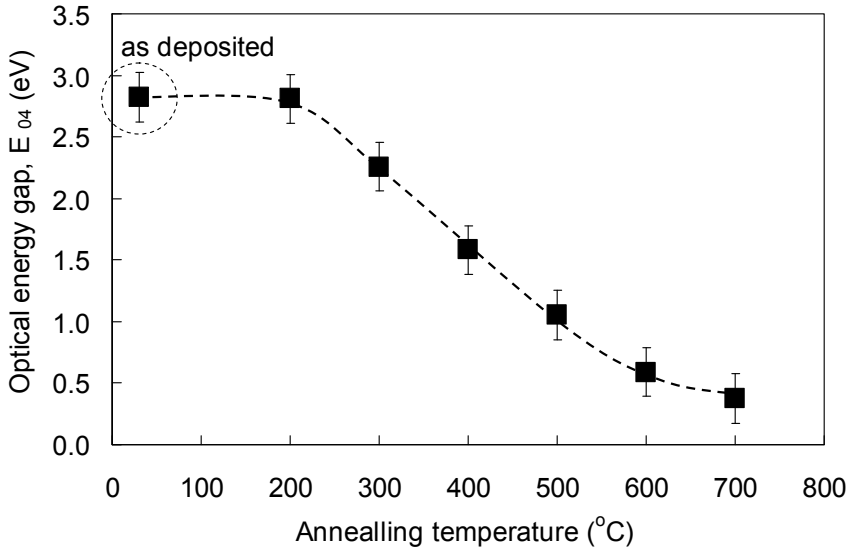

Figure 5.32: Variation of optical energy gap as a function of annealing temperature. Line is as guide to the eye.

The variation in their reflective index could not be calculated from the optical spectra since with the significant decrease in thickness the number of interference fringes becomes less and the calculations become less reliable. In the initial T_A range up to 200 ^oC, E_{04} remains unchanged. Above this T_A, E_{04} decreases almost linearly and begins to saturate at 600 – 700 ^oC. This result is similar to that of the variation in film thickness. However, E_{04} continues to show a consistent decrease, in contrast to the plateau seen in the film thickness within T_A of 400-500 ^oC. The decrease in E_{04} could be explained by the graphitization of the film as seen from FTIR. This is in line with results obtained by other researchers (Bouzerar et al. 2005; Khan et al. 1999; Zhang et al. 2000). The preferential formation of C=C bonds in the film with the loss of H and N bonds in the films leads to the formation of isolated islands of sp^2 (Khan et al. 1999). Moreover, with the increase in T_A, these islands may be connected to form larger graphitic clusters in the film. As has been discussed in previous sections, the increase in these clusters increases the width of the π and π^* and thus decreases the π-π^* gap (Zhang et al. 2000).

5.4.4 Elemental composition determined by Auger electron spectroscopy (AES)

The N/C ratio for the film calculated from their AES spectra measured at selected T_A is shown in Figure 5.33. In support of the FTIR results, the N/C ratio shows a more gradual decrease when annealed up to a T_A of 400 ^oC. From 400 – 500 ^oC, a pronounced decrease in N/C is seen, after which the ratio appears to saturate. The significant decrease in N/C coincides with the proposed breaking of C=N, N-H, nitrile bonded to fused and/or isolated aromatic and isonitrile bonded to CH_3 at T_A of 500 ^oC. The saturation in N/C above 500 ^oC and the removal of the remaining isonitrile and

nitrile bonds within this region, suggest that the amount of these bonds is very small. It is also noted that the nitrogen content at T_A of 700 ^oC, although almost negligible, is still present. Indeed it is said that some highly stable carbon nitride films do not decompose unless annealed above 700 ^oC (Wang et al. 2006b)

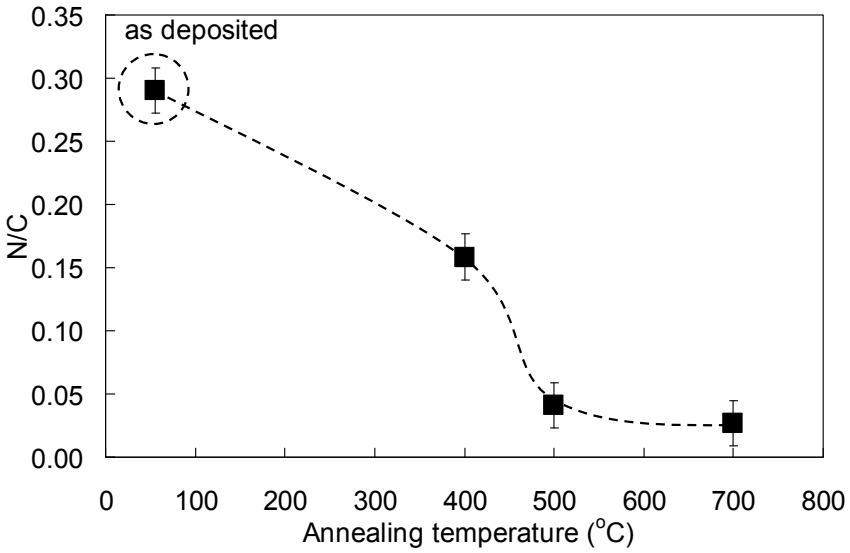

Figure 5.33: Variation of nitrogen to carbon, N/C ratio as a function of annealing temperature. Line is as guide to the eye.

5.4.5 Structural characteristics determined by Raman scattering spectroscopy

Raman scattering spectra for the p-CN_x:H as a function of T_A is shown in Figure 5.34 (a) with the baseline corrected spectra shown in Figure 5.34 (b). The latter also shows the Gaussian fittings for the spectra. The Raman spectrum of the as-deposited film shows a large contribution to the PL background which results in the slope seen for the spectrum. This is related to the high PL properties of the polymeric film. With increase in T_A this PL background decreases significantly resulting in clearer and well-defined D and G bands in these spectra. This is clearly seen from Figure 5.34 (b), where

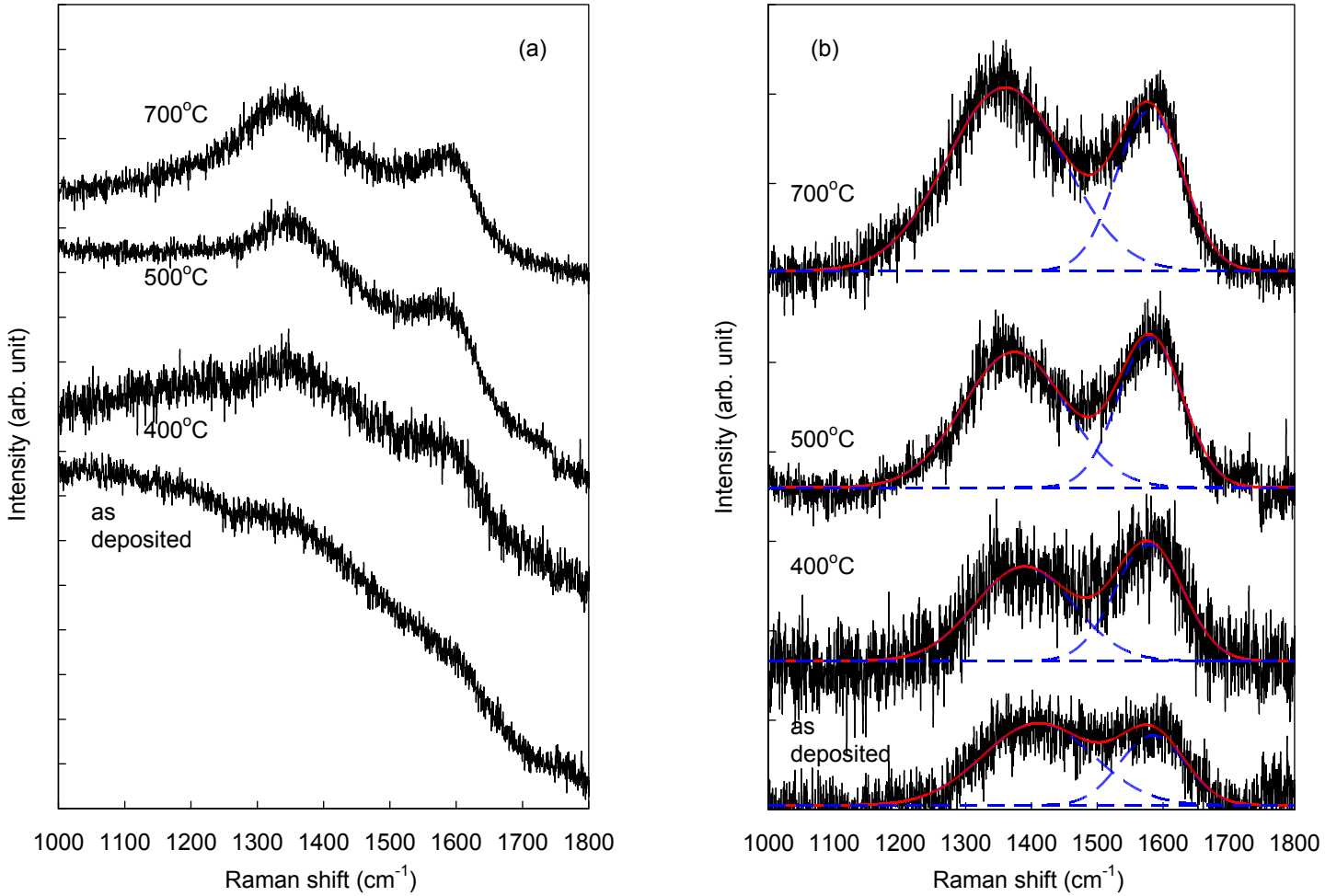

Figure 5.34: Variation in Raman scattering spectra as a function of annealing temperature, whereby (a) shows the raw data and (b) shows the deconvolution of the Raman spectra after photoluminescence background extraction.

the spectra were corrected by eliminating the PL background and were fitted using standard Gaussian fitting. The intensities of these peaks also become stronger as the samples were annealed at higher temperatures. This suggest a significant increase in sp^2 content, since for the excitation wavelength used (514 nm), these bands originates from the presence of these graphitic sp^2 bands. The increase in their intensities and thus the sp^2 content as T_A increases is in line with the proposed graphitization of the films.

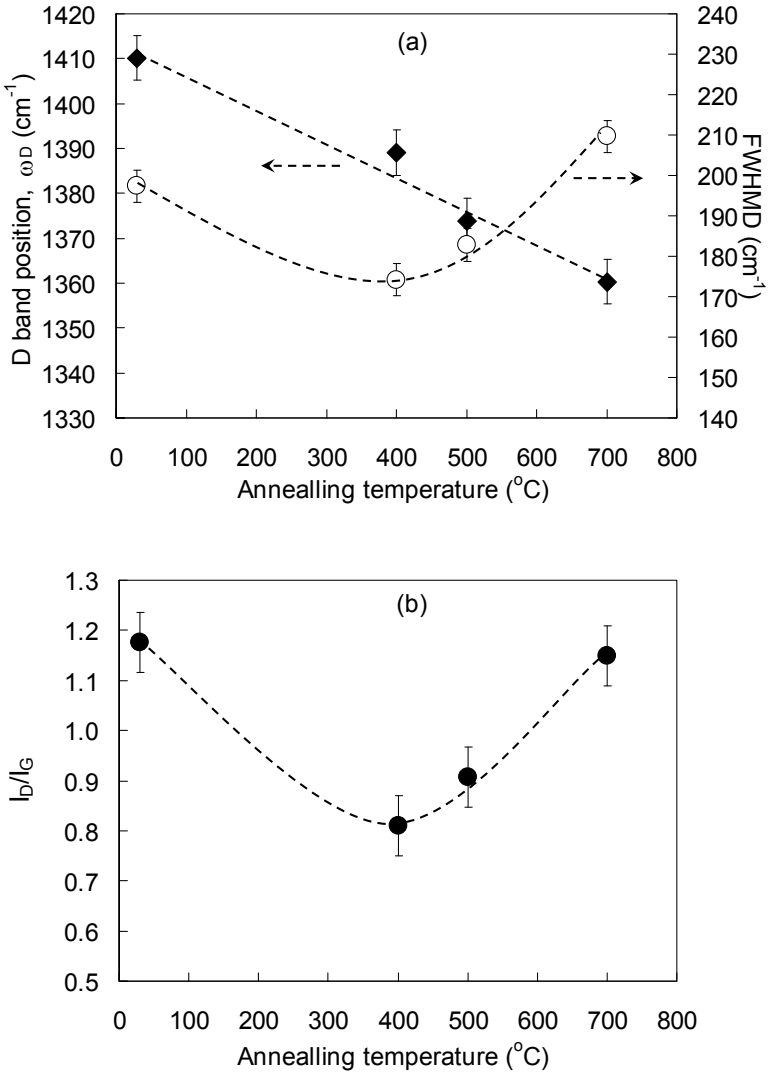

Figure 5.35: Variations in (a) peak position and width of D band, and (b) I_D/I_G, as a function of annealing temperature. Lines are as guide to the eye.

The fitting results for the position ω_D and width $FWHM_D$ of the D band, and I_D/I_G ratio are shown in Figure 5.35 (a) and (b), respectively. $FWHM_D$ and I_D/I_G ratio decrease when annealed up to T_A of 400 ^oC. Above this critical temperature these parameters increases. Although the number of data point seems insufficient for proper analysis, the trend is strongly supported by the FTIR results. The red-shift in ω_D may be attributed to the strained or curved graphite plane in the films (Li et al. 2003c; Yu et al. 2002a). With the increase in graphitic-like properties of the film at higher T_A, the presence of these graphitic planes becomes more prominent. The changes in $FWHM_D$ and the I_D/I_G ratio are strongly related to the effusion of H and N bonding in the films. The initial decrease in I_D/I_G suggests a decrease in the size of the graphitic sp^2 clusters in the film. This could be explained by the gradual loss in N bonding. For the as-deposited film the N incorporation tends to favour sp^2 units (Freire et al. 1995) and would also connect smaller sp^2 graphitic clusters in the film which results in large graphitic domains. With the loss of these N bonds the clusters breaks apart into smaller units. In contrast, the increase in the I_D/I_G ratio above the critical T_A of 400 ^oC indicates an increase in the number or size of ordered aromatic rings within the sample (Conway et al. 2000). This conversion leads to larger graphitic domains and larger sp^2 clustering (Li et al. 2003c), which coincides with the graphitization of the films.

5.4.6 Photoluminescence properties

PL spectra recorded for the as-deposited and annealed (400, 500 and 700 ^oC) films are shown in Figure 5.36. These spectra were deconvoluted by means of Gaussian fittings for the peaks corresponding to sp^2 clustering (emission energy of 2.45-2.56 eV), nitrogen bonding (3.03-3.10 eV) and the Si substrate background (3.24-3.45 eV) (Daigo

and Mutsukura 2004; Zhang et al. 1999b). The fitting results for the contribution of sp^2 clustering and N bonding in term of their variation as a function of T_A are shown in Figure 5.37 (a) and (b), respectively. Note that the PL intensity axes are plotted on a log scale for clarification. From the PL spectra in Figure 5.36 it is obvious that the decrease in the PL intensity is more drastic.

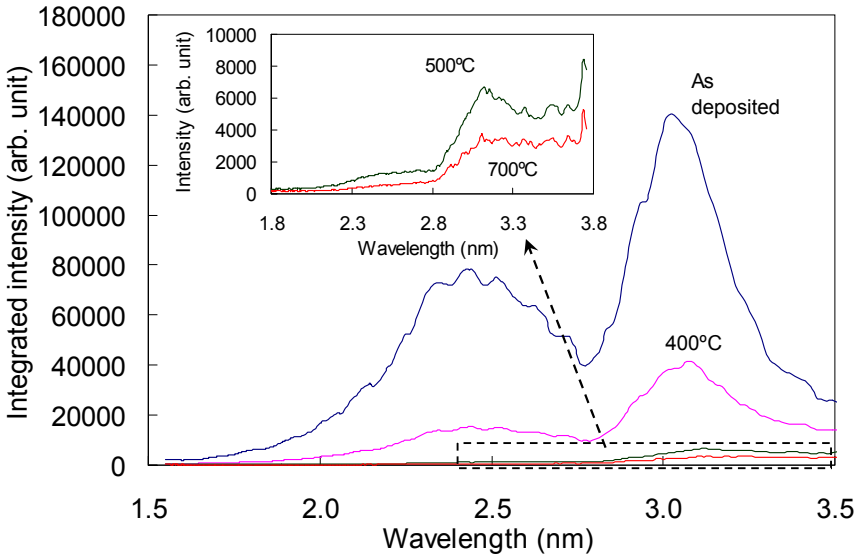

Figure 5.36: Variation in photoluminescence spectra as a function of annealing temperature. Inset show enlarged selected spectra for the annealing temperature of 500 ^{o}C and 700 ^{o}C shown for further clarification.

Both variations in PL intensities decrease significantly when annealed above 400 ^{o}C. This is in line with the graphitization of the films due to the removal of H and N- bonding. Indeed it is seen that the PL peak position also changes in accordance with the PL intensities. This correlates to the shifting in the C=C and/or C=N peak position seen in FTIR. The shifting in the photon energy of the PL emission suggests that the recombination centers have changed. The significant decrease in the PL emission also indicates an increase in non-radiative centers which dominate the recombination

processes. In general polymeric films show stronger PL characteristics than the graphitic films. The quenching of the PL with the graphitization of the film can be ascribed to the increase in states further into the gap width which creates electron-hole pairs closer to the non-radiative mid-gap defects (Conway et al. 2000). This is supported by the decrease in E_{04} of the films with increase in T_A as seen in Figure 5.32.

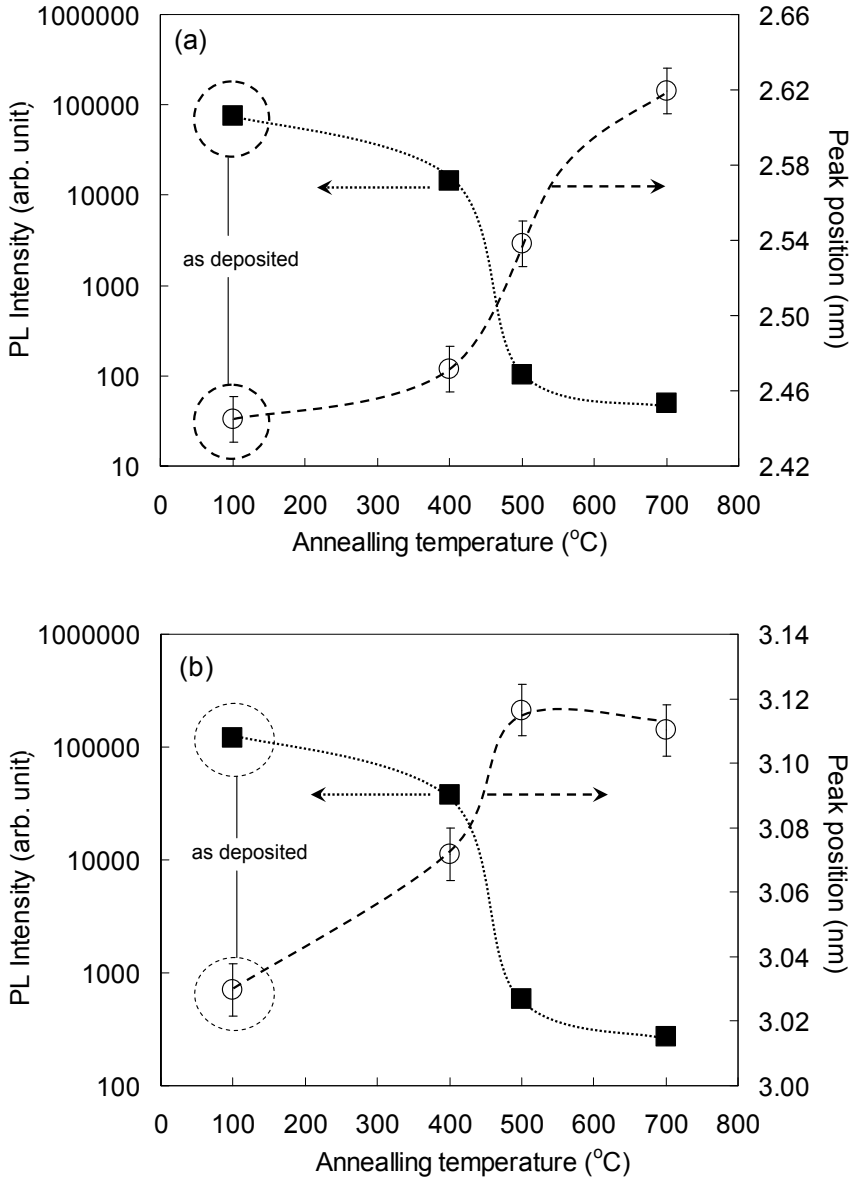

Figure 5.37: Variations of the peak intensities and positions at the photon emission range of (a) 2.45-2.56 with relation to sp^2 clustering and (b) 3.03-3.10 eV with relation to nitrogen bonding as a function of annealing temperature.

Lines are as guide to the eyes.

The quenching of the PL which coincides with the breaking of the H and N-bonds suggest these CH_n, C=N and the isolated and/or fused aromatic rings bonded to nitrile (−C≡N) may contribute significantly as recombination centers. This is deduced from the similarity of the trend in the PL intensity (Figure 5.36) and the variation in bonding characteristics (Figure 5.29). Although the contribution of CH_n in the PL properties could not be totally ignored, evidence both in this work (through the effect of applied rf power and N_2:CH_4 ratio) and those of other researchers (Mutsukura 2001), shows that the PL intensity is closely related to N bonding in the film, particularly the C≡N bonds. The contribution of the isolated and/or fused aromatic rings bonded to nitrile (−C≡N) in the formation of radiative recombination centers has been discussed in the previous studies (Section 5.3). In this section, the studies of the effect of annealing on these films suggest the C=N bonds as being yet another significant contributor to the formation of radiative recombination centers for PL emission for the p-CN_x:H films.

5.5 Summary

p-CN_x:H films were fabricated using the home-built rf PECVD system at a D_E of 5 cm. The effects of radio frequency power P_{rf}, and N_2:CH_4 ratio, together with thermal annealing, T_A on the properties of p-CN_x:H films were successfully determined. These studies were also carried out to determine their correlation with the recombination centers in these films and the optimized deposition parameters to produce high PL emission for future device fabrication. With the increase in P_{rf} the deposition rate increases and this is attributed to the increase in dissociation of the gas precursors with P_{rf}. Similar to the previous chapter, their PL emission was found to consist of a wide spectral range made up of a broad peak centered at 2.42 eV (512 nm) and a strong peak

centered at 3.05 eV (~ 407 nm). The spectral profile and thus the recombination centers remain the same regardless of P_{rf}. Indeed the constant refractive indexes, n, of the films indicate that their structure remains the same except for differences in the density of states within the film themselves. The film with the highest PL emission was obtained at P_{rf} of 80 W which has an optical band gap, E_{04} of 2.96 eV, close to the PL emission energy of the films. This is the optimized P_{rf} which gives the best conditions for radiative recombination to occur and, where the density of states in their localized centers are at their highest. This was related to the highest N content in the film at this P_{rf}. High dissociation and reaction rates as compared to etching effects due to ion bombardment promote high growth rates and N incorporation. It was also seen that the PL characteristics were dependent on the way these N atoms are bonded in the films. PL emission was enhanced by the presence of C=N and/or N–H, nitrile (bonded to aromatic rings) and isonitrile (bonded to hydrocarbon CH_3) bonds.

Films for the study of the effect of N_2:CH_4 ratio, were deposited at the optimized P_{rf} of 80 W at a D_E of 5 cm. With increase of N_2:CH_4 ratio, the film growth rate decrease which was attributed to a decrease in CH_n radicals and formation of volatile CN compounds. Both n and E_{04} decrease to a minimum at a N_2:CH_4 ratio of 0.70, indicating a change in film structure, which is in contrast to the consistency seen for P_{rf}. The film deposited at this ratio also gives the highest PL emission which increases by almost one order of magnitude compared to the other ratios. Consistent with the decrease in n and E_{04}, there is a significant shift in PL peak position at a N_2:CH_4 ratio of 0.70. Another aspect to which this study contributes (which is not seen in the study of P_{rf}) is that N incorporation itself does not directly influence the PL characteristics, but instead the way N atoms are bonded and any resulting structural changes determines their PL intensities. This study also narrows down the determining bonding for high PL

emission to the C=N, nitrile (bonded to aromatic rings) and isonitrile (bonded to hydrocarbon CH_3) bonds, excluding the contribution of N-H bonds. Also it was seen that PL was quenched by the increase in other bonding configurations of nitrile and isonitrile which act as non-radiative recombination centers. Thus, the optimized N_2:CH_4 ratio of 0.70 produced films with the strongest PL characteristics.

In the subsequent study, a film deposited at a P_{rf} of 80 W and a N_2:CH_4 ratio of 0.70, pertaining to the optimized conditions for high PL emission intensities, was subjected to thermal annealing, T_A in the temperature range of 200 °C to 700 °C. Generally, the film is thermally stable up to 500 °C. However, from 200 to 400 °C the PL intensities decrease gradually. This was attributed to the slow dissociation of N and H bonds in the films within this range, particularly in the form of CH_n and N-H. At T_A of 500 °C, both CH_n and N-H bonds totally dissociate, together with a more gradual dissociation of the nitrile and isonitrile bonds in the films. The severed bonds reconnect to form C=C bonding which induces a structural change from polymeric to graphitic-like. This also explains the decrease in E_{04} which was attributed to the formation of larger sp^2 graphitic clusters. Similarly, Raman spectroscopy supports the predicted graphitization of these films as the films shows an increase in the number and/or size of ordered aromatic rings at T_A of 500 °C and above. However, with the dissociation of these bonds, and corresponding graphitization process, PL is quenched. It was deduced from this study that CH_n bonds also contribute to the emission of PL in the films, and that the contribution of nitrile and isonitrile bonds was actually limited only to that of the isolated and/or fused aromatic rings bonded to nitrile (−C≡N).